# Highlights

## Kinetostatic Modeling of Compliant Mechanisms via Reduced-mode Cosserat Rod Model

Ke Wu, Wei Wang, Xin Li, Junzhe Hu, Pengyu Chen, Ran Cheng, Qidi Sun, Lifu Liu, Luna Zhou, Xin Xu, Shucheng Zhang, Rui Chen, Zicheng Deng, Gang Zheng

- We derive a reduced-mode Cosserat rod model.
- We simplify the model to a simple BVP of a single ODE.
- We consider bending, shear and stretch in large deflections of slender beams.
- We model large deflections of a flexible spring.
- We demonstrate advantages of the model in modeling compliant mechanisms.

# Kinetostatic Modeling of Compliant Mechanisms via Reduced-mode Cosserat Rod Model*

Ke Wu[a], Wei Wang[d], Xin Li[b], Junzhe Hu[e,f], Pengyu Chen[e,f], Ran Cheng[b], Qidi Sun[b], Lifu Liu[b], Luna Zhou[b], Xin Xu[h], Shucheng Zhang[c,g], Rui Chen[b], Zicheng Deng[g] and Gang Zheng[a,*]

[a]*INRIA Lille-Nord Europe, 40 Avenue Halley, 59650, Villeneuve d'Ascq, France.*
[b]*State Key Laboratory of Mechanical Transmission, University of Chongqing, Chongqing, 400030, China.*
[c]*LS2N - équipe ReV - Robotique Et Vivant Institut Mines Telecom Atlantique, Nantes, France*
[d]*School of Mechanical Engineering and Automation, Harbin Institute of Technology, Shenzhen 518052,P.R. China.*
[e]*Chongqing University-University of Cincinnati Joint Co-op Institute, Chongqing University, Chongqing, 400044, China.*
[f]*Center for Robotics Research, University of Cincinnati, Cincinnati, OH 45221, US.*
[g]*MIIT Key Laboratory of Dynamics and Control of Complex Systems, Northwestern Polytechnical University, Xi'an 710072, PR China*
[h]*The Hong Kong Polytechnic University (PolyU), Hongkong, China*

ARTICLE INFO

*Keywords*:
Compliant mechanisms
Large deflection
Cosserat rod theory
Model reduction
Ordinary differential equation(s)
Boundary value problem(s)

Abstract

Compliant mechanisms (CMs), which are normally composed of rigid blocks and flexible members, utilize the elastic deflection of all these built-in flexible members, to transfer motion, force and energy. In the current literature, geometrically nonlinear Euler Bernoulli beam theory and its related methods are commonly used for modeling these flexible members. However, its governing ordinary differential equation (ODE) only considers the main contributor to beam deflections: bending, without taking care of shear and axial stretch along the beam. To take care of more possible strains, Cosserat rod theory, serves as a better alternative for high accuracy. However, it still suffers from relatively complex modeling and time-consuming computation. In this paper, we propose a reduced-mode Cosserat rod model to bypass the need of conducting complex modeling, providing a more compact formulation. The detailed derivations are presented step by step, and we also propose a mode selection method to meet the requirements of different engineering scenarios. Numerical examples are provided to verify the reduced-mode model as well as the feasibility of modeling CMs. In particular, modeling flexible springs and related mechanisms has been proved valid via this proposed model.

## 1. Introduction

### 1.1. Compliant mechanisms

Compliant Mechanisms (CMs) have presented several desired properties in mechanical applications, gradually becoming a hot research area in recent years [1][2]. Different from rigid mechanisms, CMs demonstrate a new concept for energy (including force and motion) transferring that merely depends on the elastic deformation of the built-in flexible members [1][3][4]. This novel mechanism has several desired properties for mechanical applications: CMs have intrinsic compliance due to the flexibility of the used elastic material, hugely avoiding mechanical shock during operation [1]; CMs are normally designed monolithic, resulting in increased motion precision with no concerns about errors from assembly [5], and the manufacturing process is therefore simplified [1][3][5]; besides, they are light [1][3], and have less cost for manufacturing [1][3][5], and need less maintenance [1][3] compared to the rigid ones. Therefore, CMs have gradually been utilized in different mechanical applications due to these mentioned advantageous characteristics, such as compliant kinematic joints [5–7], high-accuracy positioning motion stages [8–15], bi/tri-stable mechanisms [16, 17], compliant deployable mechanisms [18–20] and other more complex applications that integrate the former three [21–23].

### 1.2. Commonly used theories and methods for modeling CMs

With the development of compliant mechanisms in applications, modeling tends to be more important in academic studies on CMs because accurate and efficient models can provide predictions in mechanical performances followed

ORCID(s):

model-based design, saving a huge amount of time in designing CMs targeting different engineering requirements [1][24]. In CMs, the most used one is geometrically nonlinear Euler Bernoulli beam theory for modeling the slender structures in CMs since its concise formulation and commonly-valid assumption which is that the deflection is purely due to bending.

To solve this beam model, there are basically two types of methods. The first one type is also the most intuitively straightforward one, called Pseudo-Rigid-Body Models (PRBMs) [1] which introduces the concept of rigid mechanisms and classic robotics, stating that a slender structure is assumed to be composed of a series of rigid links and rigid kinematic joints to behave like a Euler Bernoulli beam. In the recent literature, [25][26][27][28] utilize the basic constitutive equation of the beam theory to characterize the deflected compliant joints (flexure) based on constant-curvature assumption. We have also noticed some PRBMs that are used to characterize large deflections of slender beams under energy framework where the elastic energy is all assumed to be stored in every single passive kinematic joint, called Chained Pseudo-Rigid-Body Models (CPRBMs) [29][30]. Similar modeling methods can be found here as well: [31–38].

Besides, pioneering researchers also explore how to solve the original ordinary differential equation derived via geometrically nonlinear Euler Bernoulli beam theory, to provide more theoretical results on beam-deflection problems [1] [39][40][41]. Howell and his coworkers propose to use elliptical integral method to handle the governing equation [1]. Recently, in [39], the authors start from Lagrangian perspective to formulate the potential energy where the strain energy is totally due to bending (following the assumption of Euler Bernoulli beam theory), and use Hamilton's principle to derive its Newtonian formulation for both dynamics and statics. [40] proposed an elegant analytical solution to large-deflection problems where several assumptions are made, such as constant cross-sections and constant initial curvature. The contributors of [41] proposed a numerical solution in a very compact and clean form, to large-deflection problems of semicircular beams (with constant initial curvature), and based on the obtained results to facilitate the development of PRBMs for modeling planar compliant mechanisms.

Essentially speaking, what we need to solve regarding modeling large deflection of slender structures via geometrically nonlinear Euler Bernoulli beam theory is a typical boundary value problem (BVP) of an ordinary differential equation (ODE) [42]. Recently, some authors proposed to use typical methods for solving BVPs to handle the mentioned problem, such as finite difference method [42][43][44], shooting method [42][45], weighted residual methods [42], Taylor series method and Padé approximant [46]. Besides, a comprehensive study under Newtonian framework is presented in [24] to consider different loading conditions in CMs, such as beam-end loading, distributed loading, distributed pressure, initially varying curvature of beams, varying crosssections of beams and so on.

Euler Bernoulli beam theory has proved its effectiveness in the above mentioned cases but it still has some limitations due to its intrinsic assumption that the deflection is purely due to bending. This implies that this beam theory does not consider axial stretch and shear along the cross sections. This shortage causes some problems in modeling compliant mechanisms, such as bi-stable mechanisms [47], positioning stages [8], compliant mechanisms made of stubby flexible structures [48], and so on where the influence of axial stretch and shear can not be neglected. In the literature of CMs, there are some contributions that take care of axial stretch and shear. For example, Awtar proposed a simple, clear and also analytical formulation (termed as Beam Constraint Model) to model intermediate-range deflection where bending and axial stretch are both considered, serving as a good tool of modeling intermediate-range deflections in high-precision flexure-based motion stages [8]. Then, Guimin and Fulei extended Awtar's work by further taking care of the shear in the crosssections of beams [48], terming the new model as Timoshenko Beam Constraint Model. Therefore, this model takes care of bending, stretch and shear within intermediate-range deflection. Besides, chained Beam Constrained Models (CBCM) used for modeling large deflections [49][50] were proposed where logically the stretch and bending are both considered. In 2023, [47] added Timoshenko coefficient and elastic assumption for axial stretch to model large deflection of slender beams, and this model performs better in modeling bi-stable mechanisms compared to geometrically nonlinear Euler Bernoulli beam theory. However, Timoshenko coefficient essentially is engineering approximation, and it may cause some errors modeling different beams with cross sections [51].

Besides, we can also choose Cosserat rod theory [52][53] to model compliant mechanisms where bending, stretch and shear are all considered. However, it has not been widely used in CMs [4][24][42][54] since it is relatively complex in terms of modeling and implementation in coding, which is not as easy-to-implement as geometrically nonlinear Euler Bernoulli theory. In Cosserat rod theory, the model is written as a boundary value problem of a set ordinary differential equations with variables defined in Lie group whereas in geometrically nonlinear Euler Bernoulli theory, the model is much simpler where we just need to face a boundary value problem of just one single ordinary differential

equation defined in vector space. Besides, among all the current designs of CMs in the literature [54], planar deflections of slender structures is the most studied area so using a 3D-deflection beam theory (such as Cosserat rod model) to model 2D-deflection problems is an option but not the best one obviously. Therefore, summarizing all the needs in modeling compliant mechanisms, in this paper, we derive a reduced-mode Cosserat rod static model to consider planar large deflections of slender beams where bending, shear and stretch are all considered. In this reduced-mode model, bypassing the need of working Lie group and a set of complex ordinary differential equations, we just need to solve a simple BVP of an ODE that governs the large deflections of a slender beam. Mathematically speaking, one of our key contributions lies in reducing the number of functions to be approximated by canceling rotation matrix defined in Lie group and utilizing the orientation function to represent three strain functions (bending, shear and stretch), leading to the fact that just a simple BVP of an ODE needs to be solved where only one function is unknown. Then, we can directly use the same methods used for solving geometrically nonlinear Euler Bernoulli beam theory to handle the proposed model, such as weighted residual methods [42], which has already been proved efficient and accurate. Besides, we also present the modeling strategy of flexible springs via this proposed model, as well as the spring-based mechanisms, to demonstrate its potential of modeling different flexible structures.

### 1.3. Structure of the paper

In the following of the paper, we first recall geometrically nonlinear Euler Bernoulli beam theory and Cosserat rod theory for readers. Second, the detailed derivation of model reduction for Cosserat rod theory is presented. Then, we compare the proposed reduced-mode Cosserat rod model with the existing commonly-used methods in CMs regarding modeling single flexible structures, straight beams, pre-curved beams and flexible structures where six standards, such as time expense, accuracy, strain considerations and so on, are used to evaluate all the modeling methods. Finally, modeling CMs using this reduced-mode Cosserat rod model is studied where three types of typical mechanisms are presented: parallelograms, bi-stable mechanisms and spring-based mechanisms.

## 2. Recall of theory and prerequisites

### 2.1. Geometrically nonlinear Euler Bernoulli beam theory

The famous geometrically nonlinear Euler Bernoulli beam theory is recalled here, and it is commonly used to model large deflections of slender flexible structures in compliant mechanisms [24][55]. Here, as shown in Fig. 1, we present a typical case where a pre-curved beam (initially curved beam) is subjected to beam-end loading conditions ($F_x$, $F_y$, $M_o$), which yields the following boundary value problem of an ordinary differential equation [42]:

$$\begin{aligned} &\text{D.E.} \quad \frac{\mathrm{d}^2\theta}{\mathrm{d}s^2} = -\frac{F_y}{EI}\cos\theta(s) - \frac{F_x}{EI}\sin\theta(s) + \frac{\mathrm{d}\kappa_o}{\mathrm{d}s}(s) \\ &\text{B.C.} \quad \theta(0) = 0 \\ &\qquad \frac{\mathrm{d}\theta}{\mathrm{d}s}(L) = \frac{M_o}{EI} + \kappa_o(L) \end{aligned} \tag{1}$$

where $\kappa_o$ refers to the initial curvature of the slender beam, and $R$ refers to the radius of curvature the slender beam. They have the following relationship:

$$\kappa_o(s) = \frac{1}{R(s)} \tag{2}$$

To characterize the deformed beam shape, we have the following:

$$x(s) = \int_0^s \cos\theta(\xi)\mathrm{d}\xi;\ y(s) = \int_0^s \sin\theta(\xi)\mathrm{d}\xi \tag{3}$$

and the stored energy can be calculated via

$$E_p = \int_0^L \frac{1}{2} EI(\frac{\mathrm{d}\theta}{\mathrm{d}s})^2\mathrm{d}s \tag{4}$$

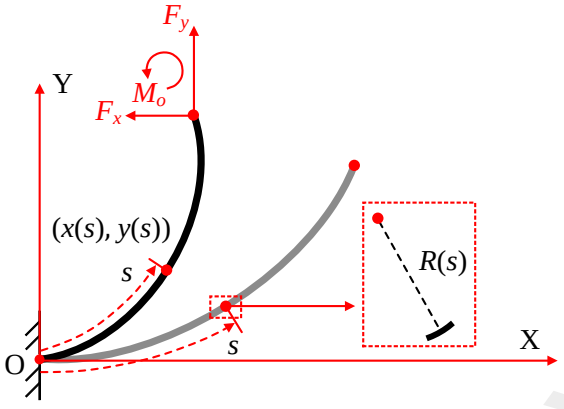


**Figure 1:** A pre-curved slender beam subjected to beam-end loading conditions

In Section 3 of this paper, we are going to compare the proposed reduced-mode Cosserat rod model and this Euler Bernoulli beam model, so we reveal the mathematical essence of the models by nondimensionalizing their governing equations for comparison. Therefore, nondimensionalizing (1) to (4), we will be able to derive the following [46]:

$$\begin{aligned} &\text{D.E.} \quad \frac{\mathrm{d}^2\hat{\theta}}{\mathrm{d}\hat{s}^2} = -f_y \cos\hat{\theta}(\hat{s}) - f_x \sin\hat{\theta}(\hat{s}) + \frac{\mathrm{d}\hat{\kappa}_o}{\mathrm{d}\hat{s}}(\hat{s}) \\ &\text{B.C.} \quad \hat{\theta}(0) = 0 \\ &\qquad \frac{\mathrm{d}\hat{\theta}}{\mathrm{d}\hat{s}}(1) = m_o + \hat{\kappa}_o(1) = m_o + \frac{1}{r(1)} \end{aligned} \tag{5}$$

where

$$f_x = \frac{F_x L^2}{EI};\ f_y = \frac{F_y L^2}{EI};\ m_o = \frac{M_o L}{EI};\ \hat{\kappa}_o(\hat{s}) = L\kappa_o(s);\ r(\hat{s}) = \frac{R(s)}{L};\ \hat{\kappa_o}(\hat{s}) = \frac{1}{r(\hat{s})};\ \hat{s} \in [0,1];\ s \in [0,L] \tag{6}$$

The normalized coordinates of the deformed beam shapes can be calculated via

$$\hat{x}(\hat{s}) = \int_0^{\hat{s}} \cos(\hat{\theta}(\xi))\mathrm{d}\xi;\ \hat{y}(\hat{s}) = \int_0^{\hat{s}} \sin(\hat{\theta}(\xi))\mathrm{d}\xi \tag{7}$$

and we can calculate the normalized stored energy through

$$\hat{E}_p = \int_0^1 \frac{1}{2}(\frac{\mathrm{d}\hat{\theta}}{\mathrm{d}\hat{s}})^2 \mathrm{d}\hat{s} \tag{8}$$

As shown in presented in (5) to (7), all variables are normalized. In essence, BVP (5) governs all large-deflection scenarios of slender beams with initial curvature under beam-end loading conditions via this nondimensionalization framework.

## 2.2. Cosserat rod theory

Cosserat rod theory is an effective tool to model large spatial deflections of elastic rods [52]. The staitc model is defined as a boundary value problem of a set ordinary differential equations defined in Lie group, and it contains three groups of equations: geometrical-compatibility equations, equilibrium equations and constitutive equations.

### *2.2.1. Geometrical compatibility*

As shown in Fig. 2, any section along a Cosserat rod can be described by $\mathrm{r}(s)$ and $\mathbf{R}(s)$ where $\mathbf{R}(s) = [\mathbf{d_1}, \mathbf{d_2}, \mathbf{d_3}]$. Note that $\mathbf{d_i}$ is a unit vector where $i = 1, 2, 3$. The important assumption that each cross section behaves as a rigid body is reflected by the fact that in Cosserat rod, the angle between $\mathbf{d_2}$ and $\mathbf{d_3}$ remains constant. Normally, we set

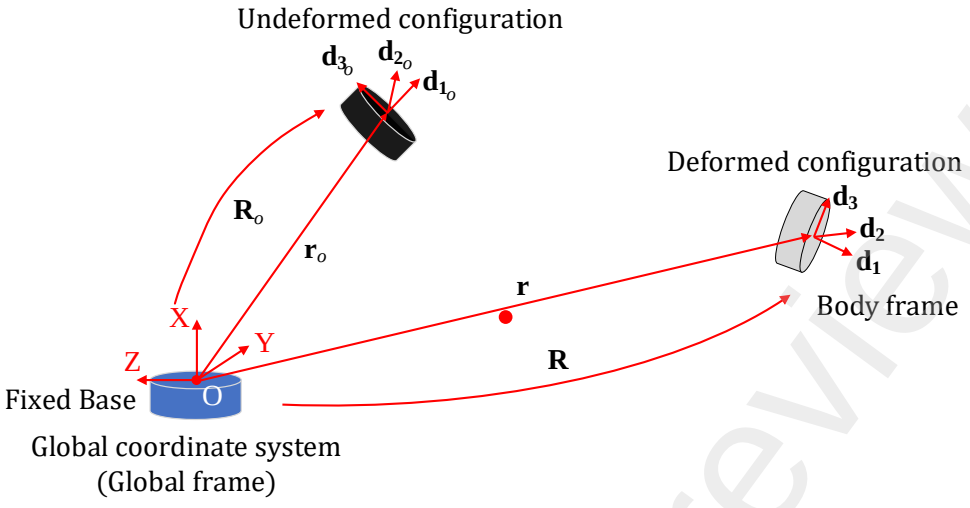


**Figure 2:** Geometrical compatibility of a Cosserat rod

$\mathbf{d_2}$ and $\mathbf{d_3}$ orthogonal to each other, and then $\mathbf{d_1}$ is defined as another orthogonal vector to both $\mathbf{d_2}$ and $\mathbf{d_3}$ such that $\mathbf{d_1} = \mathbf{d_2} \times \mathbf{d_3}$. In the geometrical representation, all variables depend on a parameter $s$ as the curvilinear coordinate along the rod axis of the undeformed configuration where

$$(\mathbf{r}_o(s), \mathbf{R}_o(s)), \ s \in [0, L] \tag{9}$$

denotes the undeformed/unconstrained configuration. logically, we have:

$$\frac{\partial \mathbf{r}_o}{\partial s} = \mathbf{v}_o(s); \ \frac{\partial \mathbf{R}_o(s)}{\partial s} = \hat{\mathbf{u}}_o(s)\mathbf{R}_o(s) \tag{10}$$

where $\mathbf{u}_o$ and $\mathbf{v}_o$ stand for the initial curvature and linear pre-strain of the rod respectively. $\hat{\mathbf{u}}_o(s)$ is the skew-symmetric matrix of $\mathbf{u}_o$. It represents the cross product in matrix notation such that $\mathbf{a} \times \mathbf{b} = \hat{\mathbf{a}}\mathbf{b}$; $\mathbf{a} \in \mathbb{R}^{3\times1}$, $\mathbf{b} \in \mathbb{R}^{3\times1}$. Therefore, for any vector $\mathbf{a} = [a_1, a_2, a_3]^\top$, the skew-symmetric matrix of $\mathbf{a}$ is defined as:

$$\hat{\mathbf{a}} = \begin{bmatrix} 0 & -a_3 & a_2 \\ a_3 & 0 & -a_1 \\ -a_2 & a_1 & 0 \end{bmatrix} \tag{11}$$

Then, the unstretched length of the studied rod can be calculated via:

$$L = \int_0^L |\mathbf{v}_o(s)| \mathrm{d}s \tag{12}$$

For geometrical representation of the deformed rod, we logically have the following:

$$\frac{\partial \mathbf{r}(s)}{\partial s} = \mathbf{v}(s); \ \frac{\partial \mathbf{R}(s)}{\partial s} = \hat{\mathbf{u}}(s)\mathbf{R}(s) \tag{13}$$

### *2.2.2. Equilibrium equations*

If we consider equilibrium of the rod at each cross section $s$, we have the following:

$$\frac{\partial \mathbf{n}(s)}{\partial s} = -\mathbf{f}(s); \ \frac{\partial \mathbf{m}(s)}{\partial s} = -\mathbf{l}(s) - \mathbf{v}(s) \times \mathbf{n}(s) \tag{14}$$

where $\mathbf{f}(s)$ and $\mathbf{l}(s)$ stand for the distributed forces and moments exerted on the rod expressed in global frame whereas $\mathbf{n}(s)$ and $\mathbf{m}(s)$ denote the respective internal forces and moments [52].

**Table 1**
*Basic variables defined in Cosserat rod model*

| | | | |
|---|---|---|---|
| $\mathbf{R}(s)$ | Rotation matrix | $\mathbf{r}(s)$ | Global position vector |
| $\mathbf{R}_o(s)$ | Initial Rotation matrix | $\mathbf{r}_o(s)$ | Global initial position vector |
| $\mathbf{u}(s)$ | Global curvature vector | $u(s)$ | Local curvature vector |
| $\mathbf{u}_o(s)$ | Global initial curvature vector | $u_o(s)$ | Local initial curvature vector |
| $\mathbf{v}(s)$ | Global stretch vector | $v(s)$ | Local stretch vector |
| $\mathbf{v}_o(s)$ | Global pre-stretch vector | $v_o(s)$ | Local pre-stretch vector |
| $\mathbf{n}(s)$ | Global force vector | $n(s)$ | Local force vector |
| $\mathbf{m}(s)$ | Global moment vector | $m(s)$ | Local moment vector |
| $\mathbf{f}(s)$ | Global distributed force vector | $f(s)$ | Local distributed force vector |
| $\mathbf{l}(s)$ | Global distributed force vector | $l(s)$ | Local distributed moment vector |

### *2.2.3. Constitutive equations*

Here, we proceed with a linear elasticity assumption for the constitutive relationships of the Cosserat rod:

$$n(s) = K^n(s)(v - v_o);\ m(s) = K^m(s)(u - u_o) \tag{15}$$

with the two stiffness matrices defined as:

$$K^n(s) = \begin{bmatrix} E(s)A(s) & 0 & 0 \\ 0 & G(s)A(s) & 0 \\ 0 & 0 & G(s)A(s) \end{bmatrix};\ K^m(s) = \begin{bmatrix} G(s)J_z(s) & 0 & 0 \\ 0 & E(s)I_2(s) & 0 \\ 0 & 0 & E(s)I_3(s) \end{bmatrix} \tag{16}$$

where $G(s)$, $E(s)$, $A(s)$, $I_i(s)$ (for $i = 2, 3$) and $J_z(s)$ denote respectively Shear Modulus, Young's Modulus, the cross section area, the second moment of inertia of the cross section along $\mathbf{d_i}(s)$ and the polar moment of inertia at torsional cross section's center located at the neutral fiber [52].

### *2.2.4. Problem statement: a boundary value problem*

Now, we have a set of ordinary differential equations (ODEs) that governs the spatial deflection of a rod, and they can be written in the global coordinate system (global frame):

$$\begin{aligned} &\frac{\partial \mathbf{r}(s)}{\partial s} = \mathbf{v}(s);\ \frac{\partial \mathbf{R}(s)}{\partial s} = \hat{\mathbf{u}}(s)\mathbf{R}(s) \\ &\frac{\partial \mathbf{n}(s)}{\partial s} = -\mathbf{f}(s);\ \frac{\partial \mathbf{m}(s)}{\partial s} = -\mathbf{l}(s) - \mathbf{v}(s) \times \mathbf{n}(s) \end{aligned} \tag{17}$$

which can be also written in body frame:

$$\begin{aligned} &\frac{\partial \mathbf{r}(s)}{\partial s} = \mathbf{R}(s)v(s);\ \frac{\partial \mathbf{R}(s)}{\partial s} = \mathbf{R}(s)\hat{u}(s) \\ &\frac{\partial n(s)}{\partial s} = -\mathbf{R}^\top(s)\mathbf{f}(s) - u(s) \times n(s);\ \frac{\partial m(s)}{\partial s} = -\mathbf{R}^\top(s)\mathbf{l}(s) - v(s) \times n(s) - u(s) \times m(s) \end{aligned} \tag{18}$$

with the boundary conditions:

$$\mathbf{R}(0) = \begin{bmatrix} 1 & 0 & 0 \\ 0 & 1 & 0 \\ 0 & 0 & 1 \end{bmatrix};\ \mathbf{n}(L) = \begin{bmatrix} F_x \\ F_y \\ F_z \end{bmatrix};\ \mathbf{m}(L) = \begin{bmatrix} M_x \\ M_y \\ M_z \end{bmatrix} \tag{19}$$

where the boundary conditions here refer to the ones of beam-end loading scenario just for example. Obviously, the boundary conditions need to correspond to the physical constraints in reality. Note that the above variables defined in the global coordinate system are all in bold whereas the rest are defined in the local one. Essentially, this above is a Robin boundary value problem (BVP) of a system of ODEs where the state vector is defined at one end, and its derivative is defined at the other end [56].

## 3. Reduced-mode Cosserat rod model

In some cases, such as flexure-based positioning stages and bistable mechanisms, where the axial strains of the beams of flexures can not be neglected [8], Euler Bernoulli beam theory is however not valid any more here. Different from geometrically nonlinear Euler Bernoulli beam theory that only considers planar bending, Cosserat rod theory takes care of all linear strains (two shear strains, two bending strains, one twisting strain and one axial strain) along the rod for the analysis of spatial deflections. However, in compliant mechanisms, planar beam (or flexure)-deflections are very common during their operations. Therefore, if we still stick to the original governing ODEs (17)(18), it will be too theoretically complex and computationally expensive to model planar deflections compared to Euler Bernoulli beam theory (1). Therefore, in this section, we aim to derive a more concise and simpler formulation of a reduced-mode Cosserat rod model for planar deflections to get rid of the modeling complexity of the full-mode one especially the formality of the rotation matrix $\mathbf{R}$ defined in Lie group. Then, we present a mode-selection strategy for the reduced-mode Cosserat rod model where a clear relationship between geometrically nonlinear Euler Bernoulli beam theory and Cosserat rod theory is revealed. In the end, the nondimensionalization of the reduced-mode Cosserat rod model is presented.

### 3.1. Variable transformation from local to global

First, before the detailed derivation, we need to transform the local variables to global ones to associate with the strain vectors, we manipulate the governing equations of Cosserat rod (18) by replacing all variables defined in body frame with the ones defined in the global frame via:

$$v(s) = K^n(s)^{-1}\mathbf{R}^\top(s)\mathbf{n}(s) + v_o; \;\; u(s) = K^m(s)^{-1}\mathbf{R}^\top(s)\mathbf{m}(s) + u_o \tag{20}$$

which logically yields the formulations in (21):

$$\begin{aligned}
&\frac{\partial \mathbf{r}(s)}{\partial s} = \mathbf{v}(s) = \mathbf{R}v(s) = \mathbf{R}(s)[K^n(s)^{-1}\mathbf{R}^\top(s)\mathbf{n}(s) + v_o] \\
&\frac{\partial \mathbf{R}(s)}{\partial s} = \mathbf{R}(s)\hat{u}(s) = \mathbf{R}(s)[K^m(s)^{-1}\hat{m}(s) + u_o] = \mathbf{R}(s)[K^m(s)^{-1}\hat{\mathbf{R}^\top}(s)\mathbf{m}(s) + u_o] \\
&\frac{\partial n(s)}{\partial s} = \frac{\partial \mathbf{R}^\top(s)\mathbf{n}(s)}{\partial s} = -\mathbf{R}^\top(s)\mathbf{f}(s) - [K^m(s)^{-1}\mathbf{R}^\top(s)\mathbf{m}(s) + u_o] \times \mathbf{R}^\top(s)\mathbf{n}(s) \\
&\frac{\partial m(s)}{\partial s} = \frac{\partial \mathbf{R}^\top(s)\mathbf{m}(s)}{\partial s} = -\mathbf{R}^\top(s)\mathbf{l}(s) - [K^n(s)^{-1}R^\top(s)\mathbf{n}(s) + v_o] \times \mathbf{R}^\top(s)\mathbf{n}(s) - [K^m(s)^{-1}\mathbf{R}^\top(s)\mathbf{m}(s) + u_o] \times \mathbf{R}^\top(s)\mathbf{m}(s)
\end{aligned} \tag{21}$$

Note that in statics for any $s \in [0, L]$, we have the following relationships for beam-end loading:

$$\mathbf{n}(s) = \mathbf{n}(L); \;\; \mathbf{m}(s) = \mathbf{m}(L) + (\mathbf{r}(L) - \mathbf{r}(s)) \times \mathbf{n}(L) \tag{22}$$

where

$$\mathbf{r}(s) = \begin{bmatrix} x(s) \\ y(s) \\ z(s) \end{bmatrix} \tag{23}$$

#### *3.1.1. Definition of rotation matrix*

In particular, as noticed in (21), the only unknown variable is the rotation matrix, which means the unknowns have been transformed from the strains $v(s)$ and $u(s)$ to $\mathbf{R}(s)$. Therefore, according to Weierstrass's first theorem, we can proceed to define $\mathbf{R}(s)$ through the following decomposition:

$$\mathbf{R}(s) = \mathbf{R}_z(\theta(s))\mathbf{R}_y(\beta(s))\mathbf{R}_x(\alpha(s)) \tag{24}$$

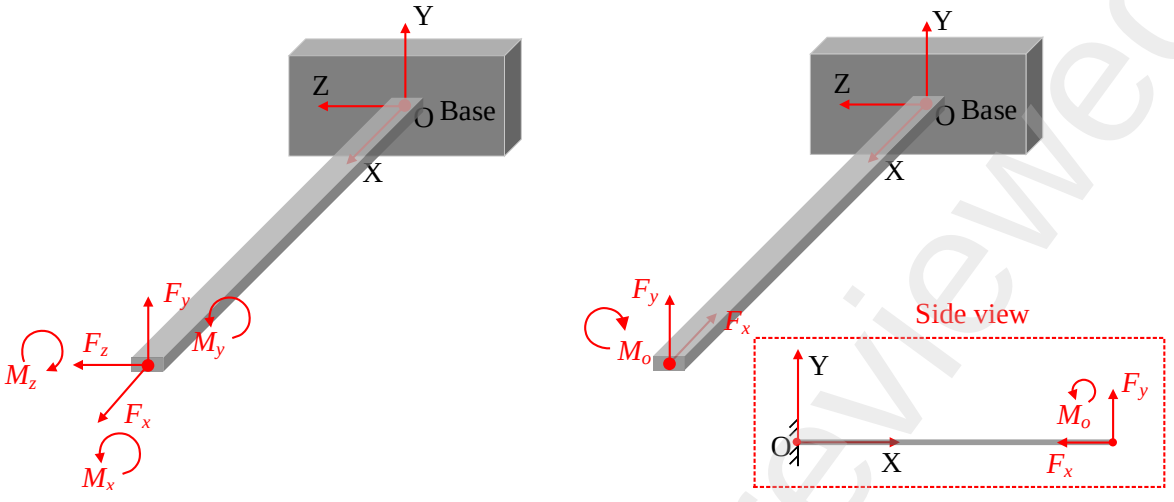


(a) A slender rod subjected to 3-D beam-end loading (b) A slender rod subjected to planar beam-end loading

**Figure 3:** Model reduction of Cosserat rod theory

where $\mathbf{R}_x(\alpha(s))$, $\mathbf{R}_y(\beta(s))$ and $\mathbf{R}_z(\theta(s))$ are defined as the rotation matrices around X, Y and Z axes respectively:

$$\begin{aligned}\mathbf{R}_x(\alpha(s)) &= \begin{bmatrix} 1 & 0 & 0 \\ 0 & \cos\alpha(s) & -\sin\alpha(s) \\ 0 & \sin\alpha(s) & \cos\alpha(s) \end{bmatrix}; \ \mathbf{R}_y(\beta(s)) = \begin{bmatrix} \cos\beta(s) & 0 & \sin\beta(s) \\ 0 & 1 & 0 \\ -\sin\beta(s) & 0 & \cos\beta(s) \end{bmatrix} \\ \mathbf{R}_z(\theta(s)) &= \begin{bmatrix} \cos\theta(s) & -\sin\theta(s) & 0 \\ \sin\theta(s) & \cos\theta(s) & 0 \\ 0 & 0 & 1 \end{bmatrix}\end{aligned} \tag{25}$$

Under this framework, $\mathbf{R}(s) \in SO3$ is always satisfied due to the formality defined.

### *3.1.2. Derivations*

As mentioned above, Cosserat rod theory can serve as an effective tool to model spatial deflections of rods taking care of bending, shear and stretch along the studied rod so planar deflections of beams can be modeled as well. However, the modeling process of planar beams would be a bit complex if we still stick to the original Cosserat rod theory. In this case, we have to directly deal with a set of ODEs like (17) and (18), which is however not necessary, because logically and also intuitively, the ODEs and vectors can be simplified into lower-dimensional ones when analyzing planar deflections. Therefore, we conduct model reduction on Cosserat rod equations from 3D to 2D deflection to consider bending, shear and stretch in planar deflections as demonstrated in Fig. 3. In Fig. 3a, the rod is subjected to spatial beam-end loading, and logically we can simplify the beam-end loading into the one that only results in planar deflections (see Fig. 3b). Supposing the studied beam is only deflected within X-O-Y plane, we can define:

$$\mathbf{r}(s) = \begin{bmatrix} x(s) \\ y(s) \\ 0 \end{bmatrix} \tag{26}$$

Logically, the boundary condition of the beam-end loading (19) can be simplified:

$$\mathbf{n}(L) = \begin{bmatrix} -F_x \\ F_y \\ 0 \end{bmatrix}; \ \mathbf{m}(L) = \begin{bmatrix} 0 \\ 0 \\ M_o \end{bmatrix} \tag{27}$$

where the minus sign in $-F_x$ is added here for coinciding with the coordinate system used to explain geometrically nonlinear Euler Bernoulli beam theory (see Fig. 1 and Fig. 3b). Similarly, the bending of the studied beam only

happens around Z axis so the rotation matrix can be formulated as:

$$\mathbf{R}(s) = \mathbf{R}_z(\theta(s))\mathbf{R}_y(\beta(s))\mathbf{R}_x(\alpha(s)) = \mathbf{R}_z(\theta(s))\begin{bmatrix}1&0&0\\0&1&0\\0&0&1\end{bmatrix}\begin{bmatrix}1&0&0\\0&1&0\\0&0&1\end{bmatrix} = \mathbf{R}_z(\theta(s)) \tag{28}$$

Therefore, the other boundary condition (19) at the fixed end yields:

$$\mathbf{R}_z(\theta(0)) = \begin{bmatrix}\cos\theta(0) & -\sin\theta(0) & 0\\ \sin\theta(0) & \cos\theta(0) & 0\\ 0 & 0 & 1\end{bmatrix} = \begin{bmatrix}1&0&0\\0&1&0\\0&0&1\end{bmatrix} \tag{29}$$

Obviously, the constraint at the fixed can be simplified as:

$$\theta(0) = 0 \tag{30}$$

Note that the initial strain and curvature set for straight beams are as follows:

$$v_0 = \begin{bmatrix}1\\0\\0\end{bmatrix};\ u_0 = \begin{bmatrix}0\\0\\\kappa_o(s)\end{bmatrix} \tag{31}$$

so we can obtain the following via (20) and (31):

$$v(s) = \begin{bmatrix}\frac{\sin\theta(s)F_y - \cos\theta(s)F_x}{A(s)E(s)} + 1\\ \frac{\cos\theta(s)F_y + \sin\theta(s)F_x}{A(s)G(s)}\\ 0\end{bmatrix};\ u(s) = \begin{bmatrix}0\\0\\\frac{M_z + (x(L)-x(s))F_y + (x(L)-x(s))F_x}{E(s)I(s)} + \kappa_o(s)\end{bmatrix} = \begin{bmatrix}0\\0\\\frac{\mathrm{d}\theta}{\mathrm{d}s}(s)\end{bmatrix} \tag{32}$$

Then, we can formulate strain vector for planar deflections:

$$\epsilon(s) = \begin{bmatrix}\epsilon_a(s)\\ \epsilon_s(s)\\ \epsilon_b(s)\end{bmatrix} = \begin{bmatrix}\frac{\sin\theta(s)F_y - \cos\theta(s)F_x}{A(s)E(s)}\\ \frac{\cos\theta(s)F_y + \sin\theta(s)F_x}{A(s)G(s)}\\ \frac{\mathrm{d}\theta}{\mathrm{d}s}(s) - \kappa_o(s)\end{bmatrix} \tag{33}$$

Here, only beam-end loading is considered so we have

$$\mathbf{f}(s) = \begin{bmatrix}0\\0\\0\end{bmatrix};\ \mathbf{l}(s) = \begin{bmatrix}0\\0\\0\end{bmatrix} \tag{34}$$

Note that any arbitrary $\mathbf{f}(s)$ and $\mathbf{l}(s)$ can be considered as well but here we proceed with the beam-end loading conditions. Arranging (21) via (26) to (34), we will be able to arrive at (35) and (36):

$$\begin{bmatrix}\frac{\mathrm{d}x}{\mathrm{d}s}(s)\\ \frac{\mathrm{d}y}{\mathrm{d}s}(s)\\ \frac{\mathrm{d}z}{\mathrm{d}s}(s)\end{bmatrix} = \begin{bmatrix}\cos\theta(s)(\epsilon_a(s)+1) - \sin\theta(s)\epsilon_s(s)\\ \sin\theta(s)(\epsilon_a(s)+1) + \cos\theta(s)\epsilon_s(s)\\ 0\end{bmatrix};\ \begin{bmatrix}-\frac{\sin\theta(s)f_m(s)}{E(s)I(s)} & -\frac{\cos\theta(s)f_m(s)}{E(s)I(s)} & 0\\ \frac{\cos\theta(s)f_m(s)}{E(s)I(s)} & -\frac{\sin\theta(s)f_m(s)}{E(s)I(s)} & 0\\ 0 & 0 & 0\end{bmatrix} = \begin{bmatrix}0&0&0\\0&0&0\\0&0&0\end{bmatrix}$$
$$\begin{bmatrix}\frac{[\sin\theta(s)F_x + \cos\theta(s)F_y]f_m(s)}{E(s)I(s)}\\ \frac{[\cos\theta(s)F_x - \sin\theta(s)F_y]f_m(s)}{E(s)I(s)}\\ 0\end{bmatrix} = \begin{bmatrix}0\\0\\0\end{bmatrix} \tag{35}$$

and

$$(\cos\theta(s)(\epsilon_a(s)+1) - \sin\theta(s)\epsilon_s(s) - \frac{\mathrm{d}x}{\mathrm{d}s}(s))F_y + (\sin\theta(s)(\epsilon_a(s)+1) + \cos\theta(s)\epsilon_s(s) - \frac{\mathrm{d}y}{\mathrm{d}s}(s))F_x = 0 \tag{36}$$

where

$$f_m(s) = (\frac{\mathrm{d}\theta}{\mathrm{d}s}(s) - \kappa_o(s))E(s)I(s) + F_x y(s) - F_x y(L) + F_y x(s) - F_y x(L) - M_o \tag{37}$$

Concluded from (35) to (37), we can reach the following relationships

$$f_m(s) = 0 \tag{38}$$

and

$$\frac{\mathrm{d}x}{\mathrm{d}s}(s) = \cos\theta(s)(\epsilon_a(s)+1) - \sin\theta(s)\epsilon_s(s);\ \ \frac{\mathrm{d}y}{\mathrm{d}s}(s) = \sin\theta(s)(\epsilon_a(s)+1) + \cos\theta(s)\epsilon_s(s) \tag{39}$$

Here, we redefine the notation of Eq. (39) for more clarity:

$$(\frac{\mathrm{d}x}{\mathrm{d}s})_{\epsilon_{as}}(s) = \cos\theta(s)(\epsilon_a(s)+1) - \sin\theta(s)\epsilon_s(s);\ (\frac{\mathrm{d}y}{\mathrm{d}s})_{\epsilon_{as}}(s) \quad = \sin\theta(s)(\epsilon_a(s)+1) + \cos\theta(s)\epsilon_s(s) \tag{40}$$

where $\epsilon_{as}$ implies that the formulations take care of the axial strain $\epsilon_a$ and shear strain $\epsilon_s$. Differentiating (38) to eliminate the unknown constants as well as assuming the studied beam is of constant cross sections and made of isotropic material ($E(s)$, $A(s)$, $G(s)$, $J_z(s)$ and $I(s)$ are all constant within $s \in [0, L]$), we will have following ODE:

$$EI\frac{\mathrm{d}^2\theta}{\mathrm{d}s^2}(s) = -F_x(\frac{\mathrm{d}y}{\mathrm{d}s})_{\epsilon_{as}}(s) - F_y(\frac{\mathrm{d}x}{\mathrm{d}s})_{\epsilon_{as}}(s) + \frac{\mathrm{d}\kappa_o}{\mathrm{d}s}(s) \tag{41}$$

In (37), we can easily simplify the boundary condition of the beam-end loading by adding $s = L$:

$$\frac{\mathrm{d}\theta}{\mathrm{d}s}(L) = \frac{M_o}{EI} + \kappa_o(L) \tag{42}$$

Finally, together with the simplified boundary conditions (30) and (42), we will arrive the following governing BVP:

$$\begin{aligned} &\text{D.E.}\ \ EI\frac{\mathrm{d}^2\theta}{\mathrm{d}s^2}(s) = -F_x(\frac{\mathrm{d}y}{\mathrm{d}s})_{\epsilon_{as}}(s) - F_y(\frac{\mathrm{d}x}{\mathrm{d}s})_{\epsilon_{as}}(s) + \frac{\mathrm{d}\kappa_o}{\mathrm{d}s}(s) \\ &\text{B.C.}\ \ \theta(0) = 0 \\ &\qquad \frac{\mathrm{d}\theta}{\mathrm{d}s}(L) = \frac{M_o}{EI} + \kappa_o(L) \end{aligned} \tag{43}$$

To characterize the deformed beam shape, we can proceed with:

$$x(s) = \int_0^s (\frac{\mathrm{d}x}{\mathrm{d}\xi})_{\epsilon_{as}}(\xi)\mathrm{d}\xi;\ \ y(s) = \int_0^s (\frac{\mathrm{d}y}{\mathrm{d}\xi})_{\epsilon_{as}}(\xi)\mathrm{d}\xi \tag{44}$$

Via (33), the stored elastic energy in the beam can be calculated through:

$$E_p = \int_0^L \frac{1}{2}EA\epsilon_a^2 + \frac{1}{2}GA\epsilon_s^2 + \frac{1}{2}EI\epsilon_b^2\mathrm{d}s \tag{45}$$

As shown in (43), we have derived the general formulation of the reduced-mode Cosserat rod model where it is expressed as a general boundary value problem of one single oridinary differential equation to govern the large planar deflection of slender beams. Then, several different numerical methods can be used to solve this BVP, such as weighted residual methods [42]. Note that we can also use this reduced-mode Cosserat rod model to analyze bi-stable mechanisms as well [55].

### *3.1.3. Mode selection for the reduced-mode Cosserat rod model*

In the reduced-mode Cosserat rod model (43) to (45) derived in Section 3.1.2, we can easily notice that in (33) the reduced model still considers bending, shear and stretch in planar deflections of beams. However, we don't always need to take care of all strains in the deflected beam since in some applications, some of them can be neglected but some need to be considered. For instance, shear strain for stubby beams [48] and axial stretch in compliant parallelograms [8] are both important factors in modeling them. Therefore, we utilize a mode-selection strategy to switch between different modes. First, we need to add a correction term into the strain vectors to take into account or drop some specific strains.

$$v(s) = H_1[K^n(s)^{-1}\mathbf{R}^\top(s)\mathbf{n}(s)] + v_o; \;\; u(s) = H_2[K^m(s)^{-1}\mathbf{R}^\top(s)\mathbf{m}(s)] + u_o \tag{46}$$

where $H_1$ and $H_2$ are defined as matrices for choosing the desired mode. In all planar beam theories, bending serves as the main contribution in planar deflections of beams so $H_2$ is fixed as:

$$H_2 = \begin{bmatrix} 0 & 0 & 0 \\ 0 & 0 & 0 \\ 0 & 0 & 1 \end{bmatrix} \tag{47}$$

Besides, to consider the axial stretch, we have:

$$H_1 = \begin{bmatrix} 1 & 0 & 0 \\ 0 & 0 & 0 \\ 0 & 0 & 0 \end{bmatrix} \tag{48}$$

To only take care of the shear of the cross sections, we have:

$$H_1 = \begin{bmatrix} 0 & 0 & 0 \\ 0 & 1 & 0 \\ 0 & 0 & 0 \end{bmatrix} \tag{49}$$

Logically, to consider both of them, $H_1$ yields

$$H_1 = \begin{bmatrix} 1 & 0 & 0 \\ 0 & 1 & 0 \\ 0 & 0 & 0 \end{bmatrix} \tag{50}$$

Instead of using (20), we use (46) to select the strains that need to be considered for different modeling purposes. Logically, we will be able to end up with a different version of (35), (36) and (41) to (45). In this case, we do a simple example for the mode-selection strategy stated above. We set

$$H_1 = \begin{bmatrix} 0 & 0 & 0 \\ 0 & 0 & 0 \\ 0 & 0 & 0 \end{bmatrix}; \; H_2 = \begin{bmatrix} 0 & 0 & 0 \\ 0 & 0 & 0 \\ 0 & 0 & 1 \end{bmatrix} \tag{51}$$

to only consider the bending of deflected beams. Then, we will be able to end up with similar relationships as (35) and (36), which can be summarized as:

$$\begin{bmatrix} \frac{\mathrm{d}x}{\mathrm{d}s}(s) \\ \frac{\mathrm{d}y}{\mathrm{d}s}(s) \\ \frac{\mathrm{d}z}{\mathrm{d}s}(s) \end{bmatrix} = \begin{bmatrix} \cos\theta(s) \\ \sin\theta(s) \\ 0 \end{bmatrix} \tag{52}$$

$$(\frac{\mathrm{d}\theta}{\mathrm{d}s}(s) - \kappa_o)(s)I(s) + F_x y(s) - F_x y(L) + F_y x(s) - F_y x(L) - M_o = 0 \tag{53}$$

Similarly, assuming the studied beam is with constant cross sections and made of isotropic material ($E(s)$, $A(s)$, $G(s)$, $C(s)$, and $I(s)$ are all constant within $s \in [0, L]$), we can finally arrive at the following:

$$\begin{aligned} &\text{D.E. } EI(s)\frac{\mathrm{d}^2\theta}{\mathrm{d}s^2}(s) = -F_x\sin\theta(s) - F_y\cos\theta(s) + \frac{\mathrm{d}\kappa_o}{\mathrm{d}s} \\ &\text{B.C. } \theta(0) = 0 \\ &\qquad \frac{\mathrm{d}\theta}{\mathrm{d}s}(L) = \frac{M_o}{EI} + \kappa_o(L) \end{aligned}$$

with the characterization of beam shapes:

$$x(s) = \int_0^s \cos\theta(\xi)\mathrm{d}\xi; \quad y(s) = \int_0^s \sin\theta(\xi)\mathrm{d}\xi$$

and the elastic energy can be formulated as:

$$E_p = \frac{1}{2}EI\epsilon_b^2\mathrm{d}s = \frac{1}{2}EI(\frac{\mathrm{d}\theta}{\mathrm{d}s})^2\mathrm{d}s$$

It is obvious that the above equations essentially correspond to the governing equations (1)(3)(4) of geometrically nonlinear Euler Bernoulli beam theory where only bending strain is considered. Therefore, it can be logically concluded that geometrically nonlinear Euler Bernoulli beam theory is one reduced mode of Cosserat rod theory where planar bending serves as the only contribution to beam deflections.

### *3.1.4. Nondimensionalization of the reduced-mode Cosserat rod model*

Similar to geometrically nonlinear Euler Bernoulli beam theory stated in Section 2.1, the governing equations of the reduced-mode Cosserat rod theory can be nondimensionalized for better understanding of how different types of strains contribute to the final deflection as well. Therefore, the dependent variable $\theta$ and the independent variable $s$ are nondimensionalized via:

$$\hat{\theta} = \frac{\theta}{1}; \ \theta = 1\hat{\theta}; \ \hat{s} = \frac{s}{L}; \ s = L\hat{s} \tag{54}$$

where $\hat{\theta}$ and $\hat{s}$ denote the nondimensionalized $\theta$ and $s$ respectively. Similarly, we go through the same procedure for $\epsilon_a(s)$ and $\epsilon_s(s)$ in Eq. (33) and Eq. (40):

$$(\frac{\mathrm{d}\hat{x}}{\mathrm{d}\hat{s}})_{\epsilon_{as}}(\hat{s}) = \cos\hat{\theta}(\hat{s})(\hat{\epsilon}_a(\hat{s}) + 1) - \sin\hat{\theta}(\hat{s})\hat{\epsilon}_s(\hat{s}); \ (\frac{\mathrm{d}\hat{y}}{\mathrm{d}\hat{s}})_{\epsilon_{as}}(\hat{s}) \quad = \sin\hat{\theta}(\hat{s})(\hat{\epsilon}_a(\hat{s}) + 1) + \cos\hat{\theta}(\hat{s})\hat{\epsilon}_s(\hat{s}) \tag{55}$$

where

$$\hat{\epsilon}_a(\hat{s}) = \frac{f_y\sin\hat{\theta}(\hat{s}) - f_x\cos\hat{\theta}(\hat{s})}{12}\eta^2; \ \hat{\epsilon}_s(\hat{s}) = \frac{(1+\nu)(\sin\hat{\theta}(\hat{s})f_x) + \cos\hat{\theta}(\hat{s})f_y}{6}\eta^2 \tag{56}$$

$\eta$ is the slenderness ratio of the studied beam defined as $\eta = \frac{h}{L}$. Then, we can nondimensionalize (43) using (54) accordingly:

$$\begin{aligned} &\text{D.E. } \frac{\mathrm{d}^2\hat{\theta}}{\mathrm{d}\hat{s}^2} = -f_y(\frac{\mathrm{d}\hat{x}}{\mathrm{d}\hat{s}})_{\epsilon_{as}} - f_x(\frac{\mathrm{d}\hat{y}}{\mathrm{d}\hat{s}})_{\epsilon_{as}} + \frac{\mathrm{d}\hat{\kappa}_o}{\mathrm{d}\hat{s}} \\ &\text{B.C. } \hat{\theta}(0) = 0 \\ &\qquad \frac{\mathrm{d}\hat{\theta}}{\mathrm{d}\hat{s}}(1) = m_o + \hat{\kappa}_o(1) = m_o + \frac{1}{r(1)} \end{aligned} \tag{57}$$

where

$$f_x = \frac{F_xL^2}{EI}; \ f_y = \frac{F_yL^2}{EI}; \ m_o = \frac{M_oL}{EI}; \ \hat{\kappa}_o(\hat{s}) = L\kappa_o(s); \ r(\hat{s}) = \frac{R(s)}{L}; \ \hat{s} \in [0,1]; \ s \in [0, L] \tag{58}$$

To characterize the nondimensionalized beam shape, we can use the following nondimensionalized formulation via Eq. (55):

$$\hat{x}(\hat{s}) = \int_0^{\hat{s}} (\frac{\mathrm{d}\hat{x}}{\mathrm{d}\xi})_{\epsilon_{as}} \mathrm{d}\xi;\ \hat{y}(\hat{s}) = \int_0^{\hat{s}} (\frac{\mathrm{d}\hat{y}}{\mathrm{d}\xi})_{\epsilon_{as}} \mathrm{d}\xi \tag{59}$$

where $\hat{x}(\hat{s})$ and $\hat{y}(\hat{s})$ are the nondimensionalized coordinates along the beam axis. Essentially, the nondimensionalized BVP (57) governs all large deflection scenarios where different materials, different beam geometries and different loading conditions are all considered. Under this framework of nondimensionalization, all physical parameters can be represented by nondimensionalized values (such as Eq. (58) and Eq. (59)).

Again, let's take a look at the effect of $\eta$ in BVP (57). As long as the used isotropic material is settled, BVP (57) gradually converges to the following if $\eta \to 0$:

$$\begin{aligned}
&\text{D.E. } \frac{\mathrm{d}^2\hat{\theta}}{\mathrm{d}\hat{s}^2} = -(f_y \cos\hat{\theta}(\hat{s}) + f_x \sin\hat{\theta}(\hat{s})) + \frac{\mathrm{d}\hat{\kappa}_o}{\mathrm{d}\hat{s}} \\
&\text{B.C. } \hat{\theta}(0) = 0 \\
&\qquad \frac{\mathrm{d}\hat{\theta}}{\mathrm{d}\hat{s}}(1) = m_o + \hat{\kappa}_o(1) = m_o + \frac{1}{r(1)}
\end{aligned}$$

with the nondimensionalized formulation of characterizing the beam shape:

$$\hat{x}(\hat{s}) = \int_0^{\hat{s}} \cos\hat{\theta}(\xi)\mathrm{d}\xi;\ \hat{y}(\hat{s}) = \int_0^{\hat{s}} \sin\hat{\theta}(\xi)\mathrm{d}\xi$$

The above equations are exactly the nondimensionalized governing equations of geometrically nonlinear Euler Bernoulli beam theory (see Eqs. (6) to (8)). In other words, a slender beam ($\eta \to 0$) can be accurately modeled via geometrically nonlinear Euler Bernoulli beam theory where the axial and shear strains can be neglected.

## 4. Modeling large deflection of a single flexible structure

In this section, we present three cases to verify the derived reduced-mode Cosserat rod model. The first two are the typical cases in compliant mechanisms: slender beams (with and without initial curvature) subjected to beam-end loading conditions. The third one is modeling flexible springs via the proposed model, and there is no existing relevant work in the field of compliant mechanisms to the best of our knowledge. Finite element method is used for verification, and the commonly-used beam models, such as geometrically nonlinear Euler Bernoulli beam theory [57], chained beam constraint model [50], Pseudo rigid body model [29], (full-mode) Cosserat rod model [53], beam constraint model [8], Timoshenko beam constraint model [48], are compared to the proposed reduced-mode Cosserat rod model.

### 4.1. A slender beam subjected to beam-end loading conditions

Here, we first study the slender beam with no initial curvature (straight beam) subjected to beam-end loading conditions (see Fig. 1). To start with, the geometric and material parameters chosen for the studied slender beam is shown in the following:

$$E = 200 \times 10^9 \text{ Pa};\ \nu = 0.3;\ w = 0.01 \text{ m};\ h = 0.006 \text{ m};\ L = 0.25 \text{ m};\ G = \frac{E}{2(1+\nu)};\ A = wh;\ \frac{\mathrm{d}\kappa_o}{\mathrm{d}s} = 0.$$

In terms of its beam-tip loading, it is shown as follows:

Loading case 1: $F_x = 1000$ N; $F_y = 1000$ N; $M_o = 120$ N.m;

Loading case 2: $F_x = 600$ N; $F_y = 600$ N; $M_o = 80$ N.m;

Loading case 3: $F_x = 200$ N; $F_y = 200$ N; $M_o = 30$ N.m;

Loading case 4: $F_x = -200$ N; $F_y = -200$ N; $M_o = -30$ N.m;

Loading case 5: $F_x = -1000$ N; $F_y = -1000$ N; $M_o = -120$ N.m;

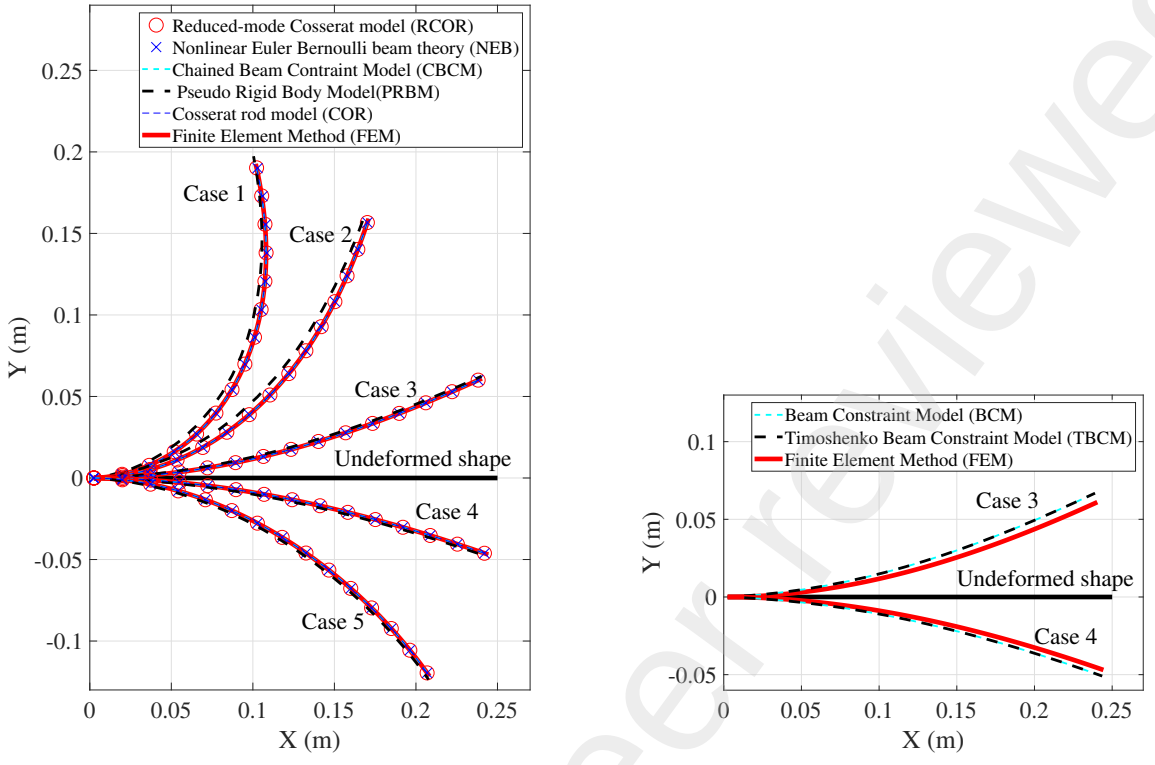


(a) Graphical results of large-range deflection of a straight slender beam

(b) Graphical results of intermediate-range deflection of a straight slender beam

**Figure 4:** Graphical results solved via different models

To both verify the accuracy and efficiency of these numerical methods, we use 3D elements under the framework of solid mechanics in finite element analysis where 60 hexahedron mesh elements are used to discretize the geometry. Besides, geometrically nonlinear Euler Bernoulli beam theory [57], chained beam constraint model [50], Pseudo rigid body model [29], (full-mode) Cosserat rod model [53], beam constraint model [8] and Timoshenko beam constraint model [48] are compared to the proposed reduce-mode Cosserat rod model here. The results are shown in Tables. 2&3 and Fig. 4.

### 4.2. A slender pre-curved beam subjected to beam-end loading conditions

In this section, we study the slender beam with initial curvature (pre-curved beam) subjected to beam-end loading conditions (see Fig. 1). The geometric and material parameters chosen for the studied slender beam is shown in the following:

$$E = 200 \times 10^9 \text{ Pa};\ \nu = 0.3;\ w = 0.01 \text{ m};\ h = 0.006 \text{ m};\ L = 0.25 \text{ m};\ G = \frac{E}{2(1+\nu)};\ A = wh;\ \frac{\mathrm{d}\kappa_o}{\mathrm{d}s} = 1000s.$$

In terms of its beam-tip loading, it is shown as follows:

Loading case 1: $F_x = 1000$ N; $F_y = 1000$ N; $M_o = 120$ N.m;

Loading case 2: $F_x = 350$ N; $F_y = 350$ N; $M_o = 50$ N.m;

Loading case 3: $F_x = -400$ N; $F_y = -600$ N; $M_o = -60$ N.m;

To both verify the accuracy and efficiency of these numerical methods, we use 3D elements under the framework of solid mechanics in finite element analysis where 51 hexahedron mesh elements are used to discretize the geometry. Besides, geometrically nonlinear Euler Bernoulli beam theory [57], (full-mode) Cosserat rod model [53], are compared to the proposed reduce-mode Cosserat rod model here. The results are shown in Table. 4 and Fig. 5.

**Table 2**
Beam-end coordinates of the deflected straight beam in the studied comprehensive case (a)

| | Case | Case 1 | Case 2 | Case 3 | Case 4 | Case 5 |
|---|---|---|---|---|---|---|
| Loading | $F_x$ (N) | 1000 | 600 | 200 | −200 | −1000 |
| | $F_y$ (N) | 1000 | 600 | 200 | −200 | −1000 |
| | $M_o$ (N.m) | 120 | 80 | 30 | −30 | −120 |
| RCOR | $x(L)$ (m) | 0.1020 | 0.1709 | 0.2404 | 0.2443 | 0.2083 |
| | $y(L)$ (m) | 0.1930 | 0.1590 | 0.0611 | −0.0470 | −0.1220 |
| | $\theta(L)$ (rad) | 1.7907 | 1.2567 | 0.4268 | −0.3342 | −0.9573 |
| ER | $x(L)$ | 1.33% | 0.48% | 0.04% | 0.02% | 0.12% |
| | $y(L)$ | 0.57% | 0.48% | 0.64% | 0.57% | 0.70% |
| | $\theta(L)$ | 0.70% | 0.56% | 0.51% | 0.44% | 0.42% |
| NEB | $x(L)$ (m) | 0.1020 | 0.1710 | 0.2404 | 0.2444 | 0.2083 |
| | $y(L)$ (m) | 0.1930 | 0.1590 | 0.0611 | −0.0470 | −0.1220 |
| | $\theta(L)$ (rad) | 1.7859 | 1.2561 | 0.4268 | −0.3343 | −0.9569 |
| ER | $x(L)$ | 1.33% | 0.43% | 0.04% | 0.02% | 0.11% |
| | $y(L)$ | 0.57% | 0.48% | 0.62% | 0.57% | 0.70% |
| | $\theta(L)$ | 0.43% | 0.51% | 0.51% | 0.44% | 0.37% |
| CBCM | $x(L)$ (m) | 0.1020 | 0.1710 | 0.2404 | 0.2444 | 0.2083 |
| | $y(L)$ (m) | 0.1930 | 0.1590 | 0.06100 | −0.0470 | −0.1220 |
| | $\theta(L)$ (rad) | 1.7865 | 1.2562 | 0.4268 | −0.3342 | −0.9570 |
| ER | $x(L)$ | 1.33% | 0.45% | 0.04% | 0.02% | 0.11% |
| | $y(L)$ | 0.57% | 0.48% | 0.62% | 0.52% | 0.70% |
| | $\theta(L)$ | 0.47% | 0.52% | 0.51% | 0.44% | 0.39% |
| PRBM | $x(L)$ (m) | 0.1000 | 0.1699 | 0.2403 | 0.2442 | 0.2078 |
| | $y(L)$ (m) | 0.1974 | 0.1638 | 0.0624 | −0.0483 | −0.1237 |
| | $\theta(L)$ (rad) | 1.7413 | 1.2131 | 0.4166 | −0.3248 | −0.9387 |
| ER | $x(L)$ | 3.27% | 1.06% | 0.10% | 0.07% | 0.37% |
| | $y(L)$ | 2.85% | 3.54% | 2.90% | 3.42% | 2.07% |
| | $\theta(L)$ | 2.08% | 2.93% | 1.89% | 2.41% | 1.54% |
| COR | $x(L)$ (m) | 0.1021 | 0.1710 | 0.2404 | 0.2444 | 0.2082 |
| | $y(L)$ (m) | 0.1931 | 0.1591 | 0.0610 | −0.0471 | −0.1221 |
| | $\theta(L)$ (rad) | 1.7906 | 1.2566 | 0.4268 | −0.3342 | −0.9574 |
| ER | $x(L)$ | 1.33% | 0.48% | 0.04% | 0.02% | 0.12% |
| | $y(L)$ | 0.57% | 0.48% | 0.64% | 0.57% | 0.70% |
| | $\theta(L)$ | 0.70% | 0.56% | 0.51% | 0.44% | 0.42% |
| FEM | $x(L)$ (m) | 0.1034 | 0.1717 | 0.2405 | 0.2444 | 0.2085 |
| | $y(L)$ (m) | 0.1919 | 0.1582 | 0.0607 | −0.0467 | −0.1212 |
| | $\theta(L)$ (rad) | 1.7782 | 1.2497 | 0.4247 | −0.3328 | −0.9533 |
| CE (s) | RCOR | 0.02 | 0.02 | 0.02 | 0.02 | 0.02 |
| | NEB | 0.02 | 0.02 | 0.02 | 0.02 | 0.02 |
| | CBCM | 0.39 | 0.44 | 0.37 | 0.26 | 0.60 |
| | PRBM | 1.50 | 0.59 | 0.17 | 0.20 | 0.17 |
| | COR | 3.50 | 2.59 | 2.17 | 2.20 | 3.17 |
| | FEM | 14 | 12 | 7 | 5 | 8 |
| Strain | | Bending | Shear | Stretch | | |
| | RCOR | ✓ | ✓ | ✓ | | |
| | NEB | ✓ | × | × | | |
| | CBCM | ✓ | × | ✓ | **Large-range** | **deflecton** |
| | PRBM | ✓ | × | × | | |
| | COR | ✓ | ✓ | ✓ | | |
| | FEM | ✓ | ✓ | ✓ | | |

## 4.3. A slender flexible spring subjected to beam-end loading conditions

In this section, we aim to model a flexible spring under beam-end loading conditions (as shown in Fig. 6a) via the proposed reduced-mode Cosserat rod model. First, we calculate the axial stretch stiffness and bending stiffness of the studied spring according to [58][59]. Then, numerical examples are presented followed by FEM to verify the

**Table 3**
Beam-end coordinates of the deflected straight beam in the studied comprehensive case (b)

| | Case | Case 1 | Case 2 | Case 3 | Case 4 | Case 5 |
|---|---|---|---|---|---|---|
| Loading | $F_x$ (N) | 1000 | 600 | 200 | −200 | −1000 |
| | $F_y$ (N) | 1000 | 600 | 200 | −200 | −1000 |
| | $M_o$ (N.m) | 120 | 80 | 30 | −30 | −120 |
| BCM | $x(L)$ (m) | N/A | N/A | 0.2397 | 0.2441 | N/A |
| | $y(L)$ (m) | N/A | N/A | 0.0640 | −0.0482 | N/A |
| | $\theta(L)$ (rad) | N/A | N/A | 0.4392 | −0.3388 | N/A |
| ER | $x(L)$ | N/A | N/A | 0.32% | 0.10% | N/A |
| | $y(L)$ | N/A | N/A | 5.54% | 3.03% | N/A |
| | $\theta(L)$ | N/A | N/A | 3.43% | 1.79% | N/A |
| TBCM | $x(L)$ (m) | N/A | N/A | 0.2397 | 0.2441 | N/A |
| | $y(L)$ (m) | N/A | N/A | 0.0641 | −0.0482 | N/A |
| | $\theta(L)$ (rad) | N/A | N/A | 0.4392 | −0.3388 | N/A |
| ER | $x(L)$ | N/A | N/A | 0.33% | 0.10% | N/A |
| | $y(L)$ | N/A | N/A | 5.56% | 3.06% | N/A |
| | $\theta(L)$ | N/A | N/A | 3.43% | 1.81% | N/A |
| FEM | $x(L)$ (m) | N/A | N/A | 0.2405 | 0.2444 | N/A |
| | $y(L)$ (m) | N/A | N/A | 0.0607 | −0.0467 | N/A |
| | $\theta(L)$ (rad) | N/A | N/A | 0.4247 | −0.3328 | N/A |
| CE (s) | BCM | N/A | N/A | ≈ 0 | ≈ 0 | N/A |
| | TBCM | N/A | N/A | ≈ 0 | ≈ 0 | N/A |
| | FEM | N/A | N/A | 7 | 5 | N/A |
| Strain | | Bending | Shear | Stretch | | |
| | BCM | ✓ | × | ✓ | | |
| | TBCM | ✓ | ✓ | ✓ | **Intermediate-range** | **deflecton** |
| | FEM | ✓ | ✓ | ✓ | | |

proposed modeling strategy for the flexible spring. Here is the dimension of the studied flexible spring:

$$\text{Number of coils } (N_t = 50);\ \text{Coil diameter } (D_c = 0.016 \text{ m});\ \text{Wire diameter } (d_w = 0.002 \text{ m});$$

$$\text{Helix pitch } (H_p = 0.004 \text{ m});\ \text{Helix angle } (\alpha = \arctan(\frac{d_w}{D_c}) = 0.1244 \text{ rad})$$

where all the above geometric parameters are graphically explained in Fig. 6b, so the length of the flexible spring can be calculated via:

$$L = N_t \times H_p = 0.2 \text{ m}$$

The below is the material properties of the flexible spring:

$$E = 200 \times 10^9 \text{ Pa};\ \nu = 0.3;\ G = \frac{E}{2(1+\nu)}$$

#### *4.3.1. Formulation of modeling a flexible spring*

To model the flexible spring, we need to know the key possible types of deformation: axial stretch (or compression) and bending [1]. Therefore, we can modify the reduced-mode Cosserat rod model to model the flexible spring since the proposed model can be used to model axial stretch (or compression) and bending of a slender structure. According to the model selection strategy stated in Section 3.1.3. We set

$$H_1 = \begin{bmatrix} 1 & 0 & 0 \\ 0 & 0 & 0 \\ 0 & 0 & 0 \end{bmatrix};\ H_2 = \begin{bmatrix} 0 & 0 & 0 \\ 0 & 0 & 0 \\ 0 & 0 & 1 \end{bmatrix}$$

Here, we term $K_b$ and $K_s$ as the bending modulus and axial stretch modulus of the spring respectively. Starting from (37), we replace $EA$ and $EI$ with $K_s$ and $K_b$ respectively:

$$K_b \frac{\mathrm{d}\theta}{\mathrm{d}s}(s) + Py(s) - Py(L) + Fx(s) - Fx(L) - M_o = 0 \tag{60}$$

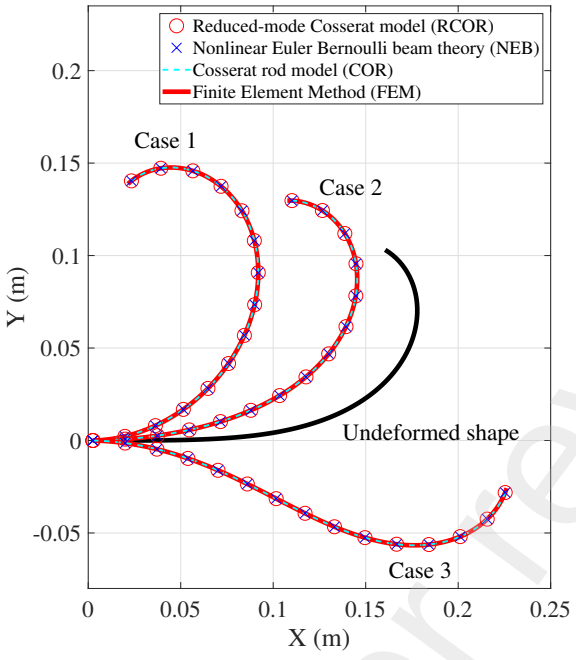


**Figure 5:** Graphical results of large-range deflection of a pre-curved beam solved via different models

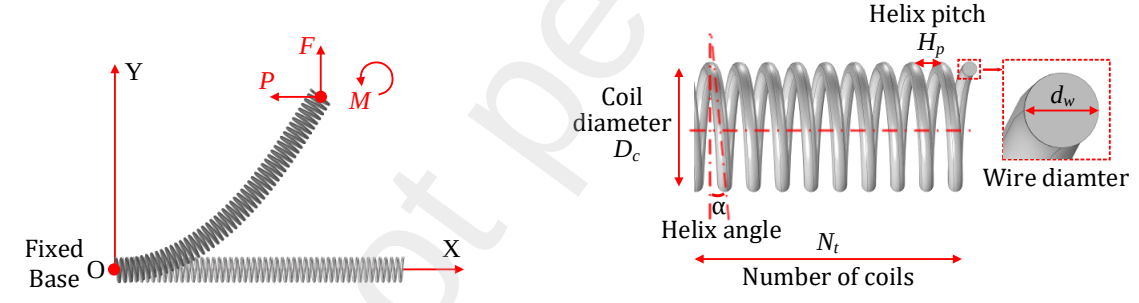


(a) The studied slender flexible spring subjected to beam-end loading conditions

(b) Detailed geometry information of the studied slender flexible spring

**Figure 6:** Demonstration of the studied slender flexible spring

Therefore, differentiating (60), we will be able to arrive at

$$\begin{aligned} &\text{D.E.} \quad \frac{\mathrm{d}^2\theta}{\mathrm{d}s^2}K_b = -P\sin\theta(s)(-\frac{\cos\theta(s)P}{K_s}+\frac{\sin\theta(s)F}{K_s}+1)-F\cos\theta(s)(-\frac{\cos\theta(s)P}{K_s}+\frac{\sin\theta(s)F}{K_s}+1)\\ &\text{B.C.} \quad \theta(0)=0\\ &\qquad \frac{\mathrm{d}\theta}{\mathrm{d}s}(L)=\frac{M}{K_b} \end{aligned} \tag{61}$$

To characterize the deformed shape of the spring, we can follow

$$x(s)=\int_0^s \cos\theta(\xi)(-\frac{\cos\theta(\xi)P}{K_s}+\frac{\sin\theta(\xi)F}{K_s}+1)\mathrm{d}\xi; \quad y(s)=\int_0^s \sin\theta(\xi)(-\frac{\cos\theta(\xi)P}{K_s}+\frac{\sin\theta(\xi)F}{K_s}+1)\mathrm{d}\xi; \tag{62}$$

Here, we first need to calculate $K_b$ and $K_s$ via the following.

**Table 4**
Beam-end coordinates of the deflected pre-curved beam in the studied comprehensive case (b)

| | Case | Case 1 | Case 2 | Case 3 |
|---|---|---|---|---|
| Loading | $F_x$ (N) | 2000 | 350 | −800 |
| | $F_y$ (N) | 1500 | 350 | −800 |
| | $M_o$ (N.m) | 120 | 50 | −100 |
| RCOR | $x(L)$ (m) | 0.0216 | 0.1077 | 0.2263 |
| | $y(L)$ (m) | 0.1388 | 0.1297 | −0.0256 |
| | $\theta(L)$ (rad) | 3.9115 | 3.1735 | 1.2760 |
| ER | $x(L)$ | 0.92% | 0.09% | 0.00% |
| | $y(L)$ | 0.07% | 0.00% | 0.79% |
| | $\theta(L)$ | 0.02% | 0.07% | 0.27% |
| NEB | $x(L)$ (m) | 0.0215 | 0.1076 | 0.2262 |
| | $y(L)$ (m) | 0.1388 | 0.1297 | −0.0258 |
| | $\theta(L)$ (rad) | 3.9146 | 3.1735 | 1.2754 |
| ER | $x(L)$ | 1.38% | 0.18% | 0.04% |
| | $y(L)$ | 0.07% | 0.00% | 1.57% |
| | $\theta(L)$ | 0.10% | 0.07% | 0.31% |
| COR | $x(L)$ (m) | 0.0215 | 0.1077 | 0.2263 |
| | $y(L)$ (m) | 0.1388 | 0.1297 | −0.0258 |
| | $\theta(L)$ (rad) | 3.9115 | 3.1735 | 1.2760 |
| ER | $x(L)$ | 1.38% | 0.09% | 0.00% |
| | $y(L)$ | 0.07% | 0.00% | 1.57% |
| | $\theta(L)$ | 0.02% | 0.07% | 0.27% |
| FEM | $x(L)$ (m) | 0.0218 | 0.1078 | 0.2263 |
| | $y(L)$ (m) | 0.1387 | 0.1297 | −0.0254 |
| | $\theta(L)$ (rad) | 3.9107 | 3.1713 | 1.2794 |
| CE (s) | RCOR | 0.02 | 0.02 | 0.02 |
| | NEB | 0.02 | 0.02 | 0.02 |
| | COR | 3.56 | 3.23 | 3.11 |
| | FEM | 14 | 9 | 7 |
| Strain | | Bending | Shear | Stretch |
| | RCOR | ✓ | ✓ | ✓ |
| | NEB | ✓ | × | × |
| | COR | ✓ | ✓ | ✓ |
| | FEM | ✓ | ✓ | ✓ |

1. **Calculation of $K_s$**
According to [58], we have the following formula for calculating the axial stiffness of a helical spring:

$$k_s = \frac{Gd_w^4}{8nD_c^3} = \frac{P}{(L - x(L))} \tag{63}$$

Then, supposing that $F = 0$, $M = 0$ and $P \neq 0$ and therefore $\theta(s) = 0$, we can rearrange (62) and (63):

$$x(L) = \int_0^L (-\frac{P}{K_s} + 1)\mathrm{d}s = L - \frac{PL}{K_s}; \tag{64}$$

Then, linking (63) with (64), we have

$$K_s = k_s L = \frac{LGd_w^4}{8nD_c^3} = 50.6637 \text{ N}; \tag{65}$$

2. **Calculation of $K_b$**
According to [59], we have the following formula for calculating the bending stiffness of a helical spring:

$$k_b = \frac{E(\frac{d_w}{2})^4 \cos\alpha}{4(2 + \nu \sin^2\alpha)n\frac{D_c}{2}} = \frac{M}{\theta(L)} \tag{66}$$

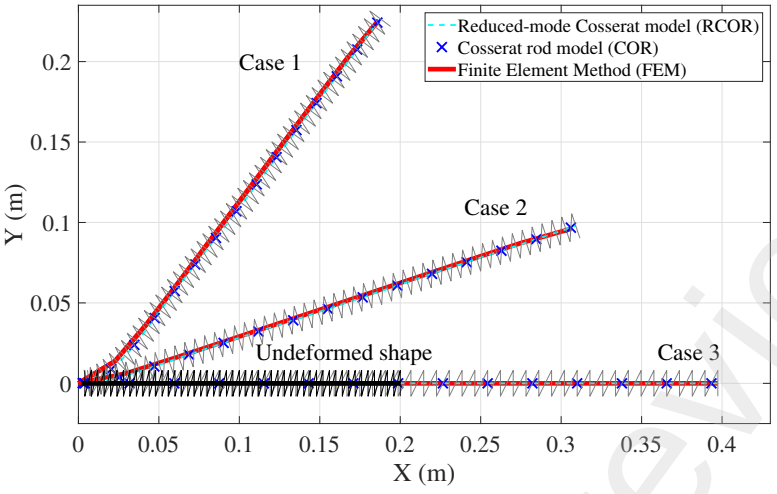


**Figure 7:** Graphical results of large-range deflection of a flexible spring solved via different models

Starting from (60) and supposing $F = 0$, $P = 0$ and $M \neq 0$, we can arrive at

$$\theta(L) = \frac{LM}{K_b} \tag{67}$$

Then, rearranging (66) and (67), we have

$$K_b = \frac{LE(\frac{d_w}{2})^4 \cos\alpha}{4(2+\nu\sin^2\alpha)n\frac{D_c}{2}} = 4.2683^{-3}\ \text{N.m} \tag{68}$$

#### *4.3.2. Numerical verification*

So far, we have obtained the axial stretch modulus $K_s$ and the bending modulus $K_b$, and then we present the following three loading cases to verify the proposed reduced-mode Cosserat rod model for modeling flexible springs.

Loading case 1: $P = -15$ N; $F = 20$ N; $M = 0$ N.m;
Loading case 2: $P = -30$ N; $F = 10$ N; $M = 0$ N.m;
Loading case 3: $P = -50$ N; $F = 0$ N; $M = 0$ N.m;

To both verify the accuracy and efficiency of these numerical methods, we use 3D elements under the framework of solid mechanics in finite element analysis where 60860 tetrahedron mesh elements are used to discretize the geometry due to the complex and irregular structure of the spring. Besides, full-mode Cosserat rod model is also compared here. The results are shown in Table. 5 and Fig. 7.

### 4.4. Results and model analysis

Regarding modeling a slender straight beam, a precurved slender beam and a flexible spring, the results of beam-end coordinates and the graphical results solved by different models are shown in Table 2 to Table 5 and Fig. 4 to Fig 7 where RCOR, NEB, CBCM, PRBM, COR, BCM, TBCM and FEM denote reduced-mode Cosserat rod model, nonlinear Euler Bernoulli beam theory [57], chained beam constraint model [50], Pseudo rigid body model [29], (full-mode) Cosserat rod model [53], beam constraint model [8], Timoshenko beam constraint model [48] and finite element method [60]. Note that ER and CE denote the error with respect to FEM and computational expense respectively.

As summarized in Table 6, all the modeling methods are evaluated regarding the following key standards: accuracy, large-deflection analysis, computational expense, strain considerations, modeling arbitrary initial curvature and modeling flexible springs. In terms of accuracy, noted from Table 2 to Table 5 and Fig. 4 to Fig 7, RCOR along with

**Table 5**
Beam-end coordinates of studied flexible spring

| | Case | Case 1 | Case 2 | Case 3 |
|---|---|---|---|---|
| Loading | $P$ (N) | −15 | −30 | −50 |
| | $F$ (N) | 20 | 10 | 0 |
| | $M$ (N.m) | 0 | 0 | 0 |
| RCOR | $x(L)$ (m) | 0.1875 | 0.3091 | 0.3973 |
| | $y(L)$ (m) | 0.2266 | 0.0978 | 0 |
| | $\theta(L)$ (m) | 0.8910 | 0.3243 | 0 |
| ER | $x(L)$ | 0.75% | 0.55% | 1.20% |
| | $y(L)$ | 0.27% | 1.56% | 0.00% |
| | $\theta(L)$ | 4.29% | 1.31% | 0.00% |
| COR | $x(L)$ (m) | 0.1879 | 0.3084 | 0.3960 |
| | $y(L)$ (m) | 0.2270 | 0.0970 | 0 |
| | $\theta(L)$ (m) | 0.8910 | 0.3242 | 0 |
| ER | $x(L)$ | 0.96% | 0.33% | 0.87% |
| | $y(L)$ | 0.44% | 0.72% | 0.00% |
| | $\theta(L)$ | 4.29% | 1.31% | 0.00% |
| FEM | $x(L)$ (m) | 0.1861 | 0.3074 | 0.3926 |
| | $y(L)$ (m) | 0.2260 | 0.0963 | 0 |
| | $\theta(L)$ (m) | 0.9322 | 0.3201 | 0 |
| CE (s) | RCOR | 2.06 | 1.86 | 0.71 |
| | COR | 10.56 | 7.23 | 7.11 |
| | FEM | > 1000 | > 1000 | > 1000 |

other modeling methods presents reliable accuracy. Is should noted that BCM and TBCM are used for intermediate-range deflection so they lose some accuracy in large-deflection analysis. As shown in Table 2 to Table 5, it can be easily noticed that PRBM, CBCM, COR and FEM require more computational time. PRBM, CBCM and FEM both depends on the number of (mesh) elements created to discretize the studied slender beam, and the more number of elements created, the more accurate results achieved. On the contrary, the more number of elements created means more equations developed so it will require more computational time. Obviously, it is a trade-off between accuracy and computational cost, so it is essential to choose the least number of elements as long as the accuracy is satisfied. It should be noted that the basic element of CBCM is BCM which is a nonlinear model for modeling intermediate-range deflection, so the number of elements needed for CBCM is less than PRBM and FEM. This is why the computational cost of CBCM is less than PRBM and FEM. Besides, BCM and TBCM share the similar closed-form formulation so their computational efficiency is also high. In terms of RCOR and NEB, they are solved via weighted residual methods [61], presenting high computational efficiency as reported in Table 2 to Table 5. For strain considerations, RCOR along with COR, TBCM and FEM takes bending, shear and stretch into account whereas other modeling methods have less strain considerations. Regarding modeling slender beams with initial curvature, all presented models are valid. However, RCOR, NEB, COR and FEM are handy to define arbitrary initial curvature via global definition of arbitrary initial curvature whereas CBCM and PRBM need to discretize the beam geometry for this same purpose [50]. Besides, TBCM and BCM are only valid for constant curvature [8][10]. Last but not the least, in the presented model only RCOR, COR and FEM can be used to model flexible springs since these models can consider large-deflection as well as the axial stretch and bending.

As analyzed above and shown in Table 6, it is obvious that RCOR have presented desired performances regarding the six evaluation standards, serving as an efficient and accurate tool modeling deflection of single slender structures. In the next section,

## 5. Modeling compliant mechanisms

In this section, we aim to verify the feasibility of modeling CMs via RCOR as well as compare RCOR with the existing commonly modeling methods. In the following, we present three cases: compliant parallelograms, bi-stable mechanisms and compliant revolute joint where RCOR all present better performances in terms of the six standards summarized in Table 6, such as more strain considerations in stubby beams in compliant parallelograms and high axial tension or compression in bi-stable mechanisms. In this section, we still follow the same denotion where RCOR, NEB, CBCM, PRBM, COR, BCM, TBCM and FEM denote reduced-mode Cosserat rod model, nonlinear Euler Bernoulli

**Table 6**
Evaluation of commonly-used modeling method for slender structures

| | RCOR | NEB | CBCM | PRBM | COR | BCM | TBCM | FEM |
|---|---|---|---|---|---|---|---|---|
| Accuracy | ✓ | ✓ | (✓) | (✓) | ✓ | (✓) | (✓) | ✓ |
| Large deflection | ✓ | ✓ | ✓ | ✓ | ✓ | × | × | ✓ |
| Computational expense | – | – | (–) | (+) | (+) | – | – | + |
| Strain considerations | 3 | 1 | 2 | 1 | 3 | 2 | 3 | > 3 |
| Arbitrary initial curvature | ✓ | ✓ | (✓) | (✓) | ✓ | (✓) | (✓) | ✓ |
| Modeling flexible springs | ✓ | × | × | × | ✓ | × | × | ✓ |

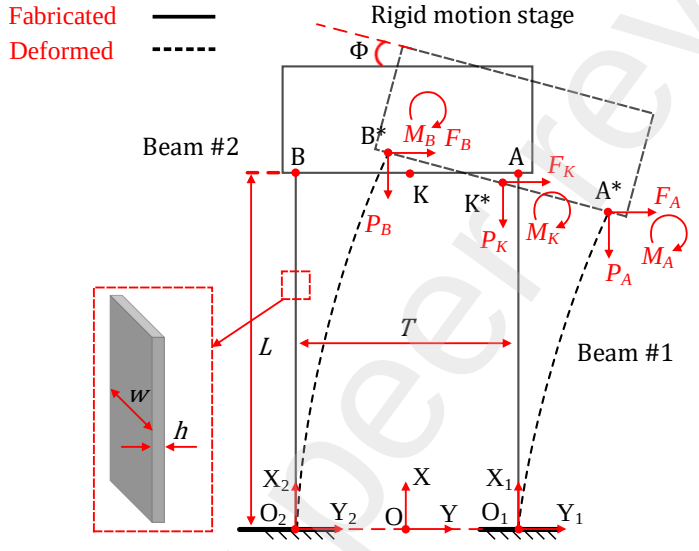


**Figure 8:** Detailed diagram of the studied compliant parallelogram

beam theory [57], chained beam constraint model [50], Pseudo rigid body model [29], (full-mode) Cosserat rod model [53], beam constraint model [8], Timoshenko beam constraint model [48] and finite element method [60].

## 5.1. Compliant parallelograms

Here, a typical CM, a straight-beam-based compliant parallelogram is studied. As shown in Fig. 8, the mechanism is composed of a rigid motion stage and two compliant beams (Beam #1 and Beam #2). $K$ is the reference point. Other geometric information and loading conditions are also provided in Fig. 8. Normally, compliant parallelograms serve as positioning stages where the built-in flexible beams are deflected to realize this function. In terms of the constitutive models for each flexible beam, RCOR is used along with NEB, TBCM and BCM for comparison, and FEM is used for verification. The static model is composed of three parts: constitutive equations, force equilibrium equations and geometric compatibility equations.

- **Static modeling**

  1) **Constitutive equations**

  For Beam #1, according to (43) and (44), we have

$$\begin{aligned} &\text{D.E.} \quad EI\frac{\mathrm{d}^2\theta_1}{\mathrm{d}s^2}(s) = -P_A(\frac{\mathrm{d}y_1}{\mathrm{d}s})_{\epsilon_{as}}(s) - F_A(\frac{\mathrm{d}x_1}{\mathrm{d}s})_{\epsilon_{as}}(s) \\ &\text{B.C.} \quad \theta_1(0) = 0 \\ &\qquad \frac{\mathrm{d}\theta_1}{\mathrm{d}s}(L) = \frac{M_A}{EI} \end{aligned} \tag{69}$$

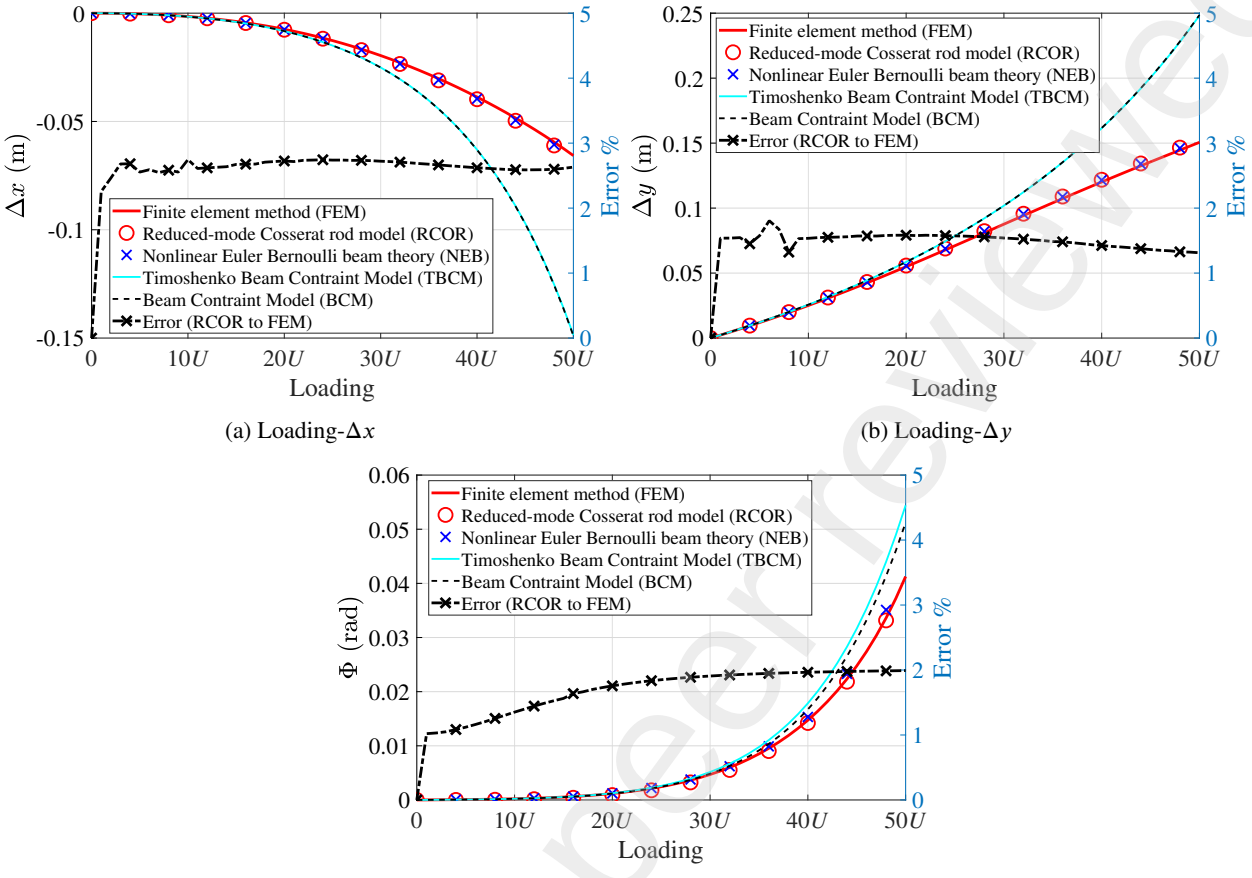


(a) Loading-$\Delta x$

(b) Loading-$\Delta y$

(c) Loading-$\Phi$

**Figure 9:** Numerical results of the studied compliant parallelogram with slender beams

and

$$x_1(s) = \int_0^s (\frac{\mathrm{d}x_1}{\mathrm{d}\xi})_{\epsilon_{as}}(\xi)\mathrm{d}\xi;\ y_1(s) = \int_0^s (\frac{\mathrm{d}y_1}{\mathrm{d}\xi})_{\epsilon_{as}}(\xi)\mathrm{d}\xi \tag{70}$$

For Beam #2, similarly, we have

$$\begin{aligned} &\text{D.E. } EI\frac{\mathrm{d}^2\theta_2}{\mathrm{d}s^2}(s) = -P_B(\frac{\mathrm{d}y_1}{\mathrm{d}s})_{\epsilon_{as}}(s) - F_B(\frac{\mathrm{d}x_2}{\mathrm{d}s})_{\epsilon_{as}}(s) \\ &\text{B.C. } \theta_2(0) = 0 \\ &\qquad \frac{\mathrm{d}\theta_2}{\mathrm{d}s}(L) = \frac{M_B}{EI} \end{aligned} \tag{71}$$

and

$$x_2(s) = \int_0^s (\frac{\mathrm{d}x_2}{\mathrm{d}\xi})_{\epsilon_{as}}(\xi)\mathrm{d}\xi;\ y_2(s) = \int_0^s (\frac{\mathrm{d}y_2}{\mathrm{d}\xi})_{\epsilon_{as}}(\xi)\mathrm{d}\xi \tag{72}$$

2) **Force equilibrium equations**

$$\begin{aligned} &F_K - F_A - F_B = 0;\ P_K - P_A - P_B = 0 \\ &M_K - M_A - M_B + F_K T/2\sin\Phi - P_K T/2\cos\Phi - F_B T\sin(\Phi) + P_B T\cos(\Phi) = 0 \end{aligned} \tag{73}$$

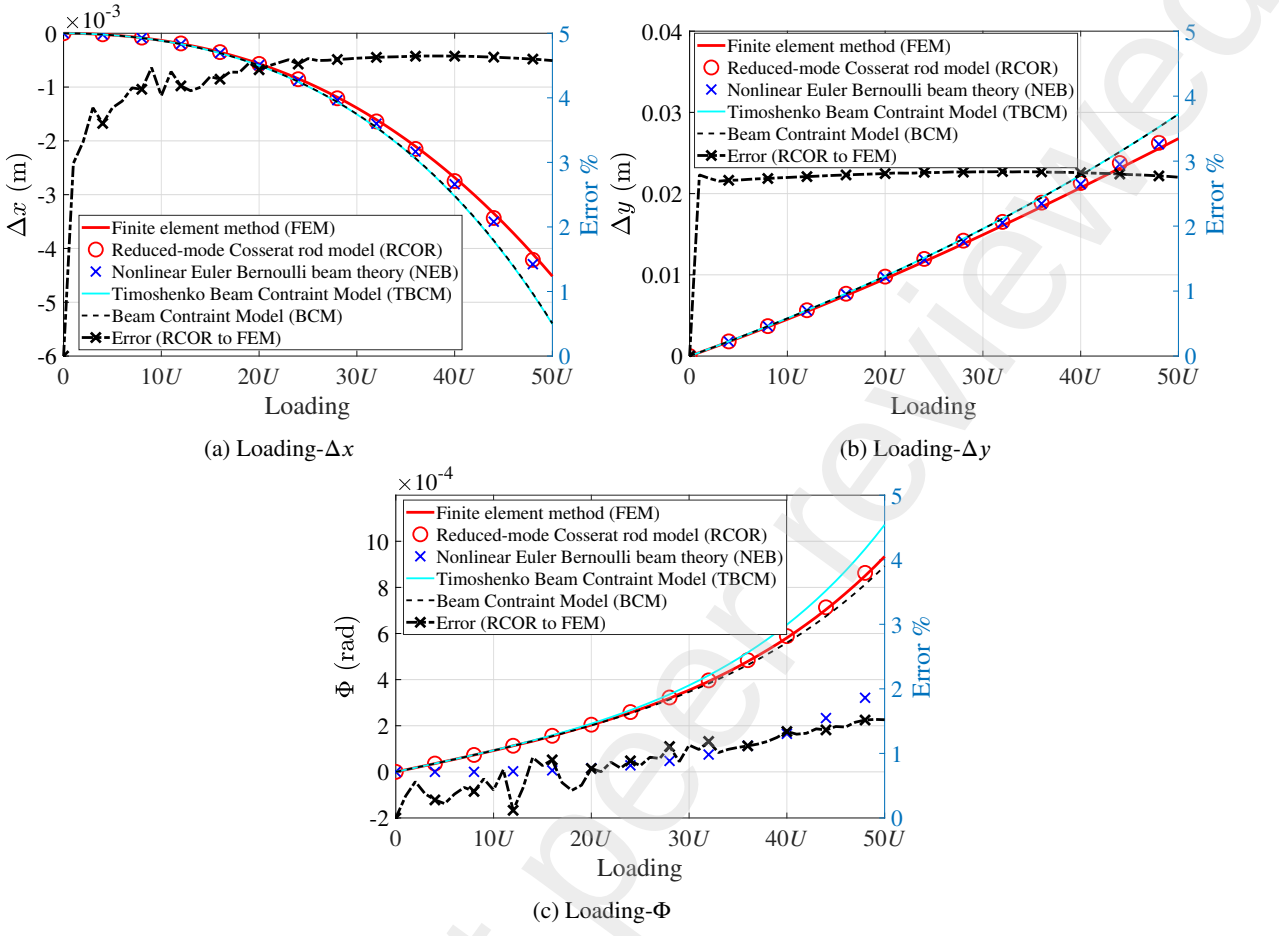


(a) Loading-$\Delta x$ (b) Loading-$\Delta y$

(c) Loading-$\Phi$

**Figure 10:** Numerical results of the studied compliant parallelogram with stubby beams

3) **Geometric compatibility equations**

$$
\begin{aligned}
&\begin{bmatrix} x_A \\ y_A \end{bmatrix} = \begin{bmatrix} L \\ T/2 \end{bmatrix};\ \begin{bmatrix} x_{A^*} \\ y_{A^*} \end{bmatrix} = \begin{bmatrix} \int_0^L \cos\theta_1(s)\mathrm{d}s \\ \int_0^L \sin\theta_1(s)\mathrm{d}s \end{bmatrix} + \begin{bmatrix} 0 \\ T/2 \end{bmatrix};\\
&\begin{bmatrix} x_B \\ y_B \end{bmatrix} = \begin{bmatrix} L \\ -T/2 \end{bmatrix};\ \begin{bmatrix} x_{B^*} \\ y_{B^*} \end{bmatrix} = \begin{bmatrix} \int_0^L \cos\theta_2(s)\mathrm{d}s \\ \int_0^L \sin\theta_2(s)\mathrm{d}s \end{bmatrix} - \begin{bmatrix} 0 \\ T/2 \end{bmatrix};\\
&\mathrm{AB} = [(x_A - x_B)^2 + (y_A - y_B)^2]^{0.5} = T;\ \mathrm{A^*B^*} = [(x_{A^*} - x_{B^*})^2 + (y_{A^*} - y_{B^*})^2]^{0.5} = T;\\
&|x_{A^*} - x_{B^*}| = T\sin\Phi;\ |y_{A^*} - y_{B^*}| = T\cos\Phi;\ \theta_1(L) = \theta_2(L) = \Phi;\\
&\begin{bmatrix} x_K \\ y_K \end{bmatrix} = \frac{1}{2}\begin{bmatrix} x_A \\ y_A \end{bmatrix} + \frac{1}{2}\begin{bmatrix} x_B \\ y_B \end{bmatrix};\ \begin{bmatrix} x_{K^*} \\ y_{K^*} \end{bmatrix} = \frac{1}{2}\begin{bmatrix} x_{A^*} \\ y_{A^*} \end{bmatrix} + \frac{1}{2}\begin{bmatrix} x_{B^*} \\ y_{B^*} \end{bmatrix};\ \begin{bmatrix} \Delta x \\ \Delta y \end{bmatrix} = \begin{bmatrix} x_{K^*} \\ y_{K^*} \end{bmatrix} - \begin{bmatrix} x_K \\ y_K \end{bmatrix}
\end{aligned}
\tag{74}
$$

where $\begin{bmatrix} x_A & y_A \end{bmatrix}^\top$, $\begin{bmatrix} x_{A^*} & y_{A^*} \end{bmatrix}^\top$, $\begin{bmatrix} x_B & y_B \end{bmatrix}^\top$, $\begin{bmatrix} x_{B^*} & y_{B^*} \end{bmatrix}^\top$, $\begin{bmatrix} x_K & y_K \end{bmatrix}^\top$ and $\begin{bmatrix} x_{K^*} & y_{K^*} \end{bmatrix}^\top$ are the coordinates of A, A*, B, B*, K and K* in the global coordinate system X-O-Y (see Fig. 8). Then, we can numerically solve Eq. (69) to (74) using weighted residual methods [42] and Newton-Raphson method. Besides, $\begin{bmatrix} \Delta x & \Delta y & \Phi \end{bmatrix}^T$ refers to the translational and rotational displacements of K, the reference point of the modeled mechanism. For this modeling, we are interested in the relationships between applied loads $\begin{bmatrix} F_K & P_K & M_K \end{bmatrix}^T$ and the corresponding displacements $\begin{bmatrix} \Delta x & \Delta y & \Phi \end{bmatrix}^T$ both at the reference point K.

- **Mechanism analysis**
  For this above modeling via the proposed RCOR, NEB, BCM, TBCM and FEM are compared, followed by FEM validation. In the following mechanism analysis, 2 different geometries of the built-in beams are studied: stubby beams and slender beams. The material properties and geometry information (apart from the beam length $L$) are provided in the following:

$$E = 200 \times 10^9 \text{ Pa};\ \nu = 0.3;\ w = 0.015 \text{ m};\ h = 0.0045 \text{ m};\ I = \frac{wh^3}{12};\ G = \frac{E}{2(1+\nu)};\ T = 0.2 \text{ m};\ A = hw$$

  1) Slender beams ($L = 0.25$ m)
     The applied loads are set up as:

$$\begin{bmatrix} F_K \\ P_K \\ M_K \end{bmatrix} = qU = q \begin{bmatrix} 80 \text{ N} \\ 80 \text{ N} \\ 4 \text{ N.m} \end{bmatrix} \quad (q = 1, 2, 3, 4..50)$$

     The numerical results are provided in Fig. 9. In the modeling process, the next-step initial guess is set up as the last-step answer for faster convergence [60]. As shown in Fig. 9, TBCM and BCM are only valid for intermediate-range deflection so they are not correct any more as large deflection of the built-in slender beams occurs. It is shown in Fig. 9that the results of RCOR and NEB almost cover each other. This is logical because bending is the largest contributor in large deflection of slender beams whereas stretch and shear considered by RCOR don not matter that much in this case.
  2) Stubby beams ($L = 0.1$ m)
     The applied loads are set up as:

$$\begin{bmatrix} F_K \\ P_K \\ M_K \end{bmatrix} = qU = q \begin{bmatrix} 240 \text{ N} \\ 240 \text{ N} \\ 12 \text{ N.m} \end{bmatrix} \quad (q = 1, 2, 3, 4..50)$$

     The numerical results are provided in Fig. 10. In the modeling process, the next-step initial guess is set up as the last-step answer for faster convergence [60]. Similarly, BCM and TBCM both present accuracy within intermediate-range deflection, and become less accurate as the deflection turns larger. For modeling mechanism with stubby beams, stretch and shear turn more important in their deflections so NEB (which only considers bending) is not valid anymore, especially the rotation of the mechanism as demonstrated in Fig. 10c.

  Therefore, compared to NEB, BCM and TBCM, RCOR present reliable accuracy both in strain considerations and large-deflection analysis, which is exactly the same as concluded in Table 6. Logically, the advantages of modeling single flexible beams via RCOR have also been proved valid in modeling compliant mechanisms as well.

## 5.2. Bi-stable mechanisms

Bi-stable compliant mechanisms experience nonlinear buckling and nonlinear post-buckling when operating, which is difficult to model. In this section, a typical bi-stable compliant mechanisms is modeled where the built-in flexible members are modeled via reduced-mode Cosserat rod model (RCOR), BVP (43). This means, besides bending, the axial and shear strains are both considered. Here, NEB is used for comparisons, followed by FEM verification. As shown in Fig. 11a, the bi-stable mechanism is composed of 1 rigid motion stage and 2 flexible beams. State 1 refers to its fabricated shape where the mechanism is symmetrically fabricated and fixed at the two sides. The detailed geometric parameters are all provided in Fig. 11. The mechanism has 3 states where State 1 and State 3 are the stable equilibrium states whereas State 2 is the unstable equilibrium state. Subjected to the external force $F_o$, the mechanism works from State 1 through State 2 finally arriving at State 3. Here, we are interested in the relationship between $F_o$ and the displacement $\Delta Y$ of the reference point R. Since the structure of the bi-stable mechanism is symmetrical, we can simplify the modeling by working on the half of it as shown in Fig. 11b. We can formulate a

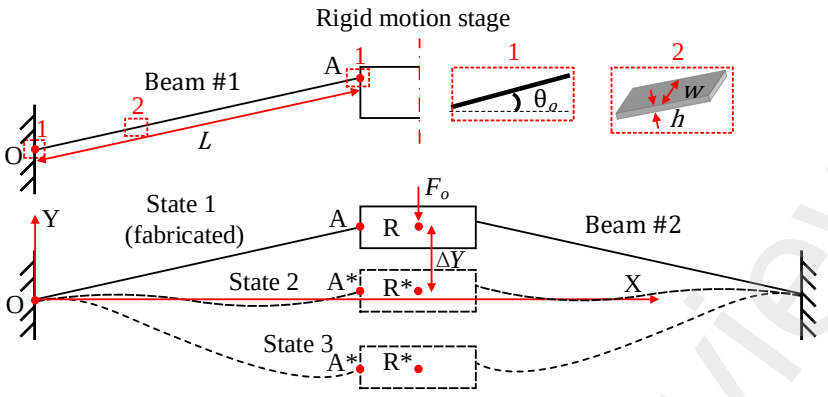


(a) Schematic diagram of a classic bi-stable compliant mechanism

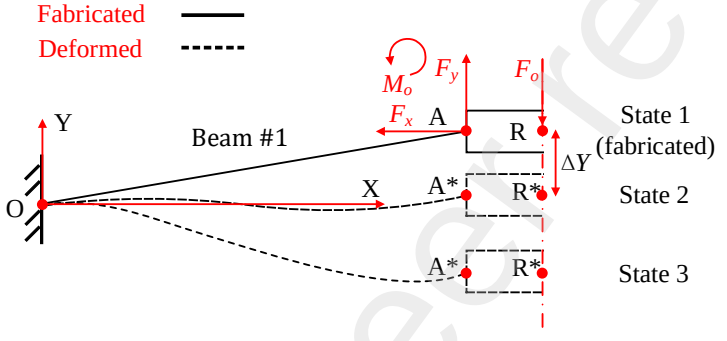


(b) Detailed force diagram of the classic compliant bi-stable mechanism

**Figure 11:** Demonstration of the studied classic compliant bi-stable mechanism

boundary value problem of an ordinary differential equation with some constraints to model this bi-stable mechanism:

$$\begin{aligned} &\text{D.E.}\quad EI\frac{\mathrm{d}^2\theta}{\mathrm{d}s^2}(s) = -F_x(\frac{\mathrm{d}y}{\mathrm{d}s})_{\epsilon_{as}}(s) - F_y(\frac{\mathrm{d}x}{\mathrm{d}s})_{\epsilon_{as}}(s) \\ &\text{B.C.}\quad \theta(0) = \theta(L) = \theta_o \\ &\qquad \frac{\mathrm{d}\theta}{\mathrm{d}s}(L) = \frac{M_o}{EI} \end{aligned} \tag{75}$$

with some constraints

$$F_o = -2F_y;\ x(L) = \int_0^L \cos\theta(s)\mathrm{d}s = L\cos\theta_o;\ \Delta Y = L\sin\theta_o - \int_0^L \sin\theta(s)\mathrm{d}s \tag{76}$$

and we can calculate the stored energy $E_p$ of the bi-stable mechanism according to (45). Then, we can numerically solve Eq. (75) and (76) using weighted residual methods [42] and Newton-Raphson method. For modeling this mechanism, we are interested in the relationship between $\Delta Y$ and $F_o \& E_p$. The material properties and geometry information are provided in the following:

$$E = 200\times10^9 \text{ Pa};\ \nu = 0.3;\ w = 0.015 \text{ m};\ h = 0.005 \text{ m};\ L = 0.25 \text{ m};$$
$$I = \frac{wh^3}{12};\ G = \frac{E}{2(1+\nu)};\ A = hw;\ \theta_o = 0.1744 \text{ rad}$$

As depicted in Fig. 12, RCOR and NEB can both capture the trend of the ground-truth results from FEM as well as the three equilibrium states (State 1 to State 3). However, RCOR is more accurate modeling the studied bi-stable

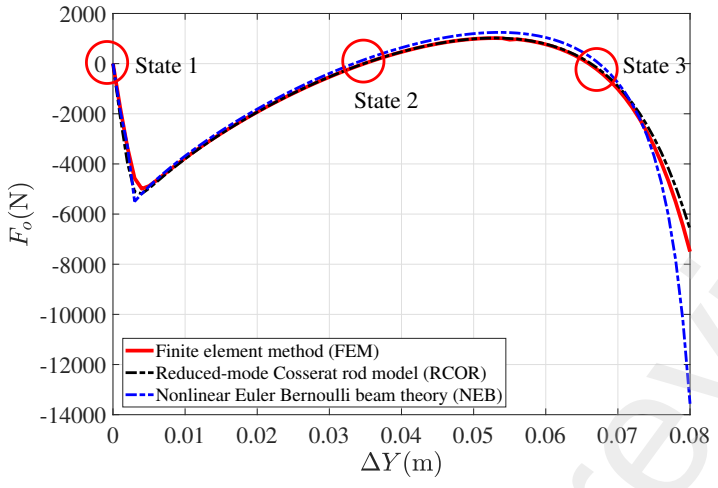


(a) $\Delta Y$-$F_o$

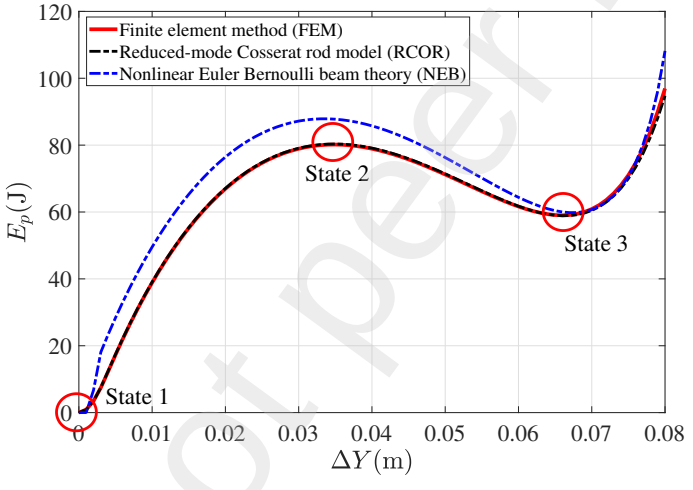


(b) $\Delta Y$-$E_p$

**Figure 12:** Numerical results of the studied bi-stable mechanism

mechanism since it considers stretch (or compression) and shear besides bending. Stretch (or compression) can not be neglected in modeling bi-stable mechanisms since the built-in beams are subjected to high axial loading, experiencing buckling and post-buckling [55]. Therefore, compare to the existing methods [54], this case study also proves the advantages of the proposed reduced-mode Cosserat rod model in modeling slender structures subjected to high axial loading.

### 5.3. Spring-based compliant translational mechanism

Flexible springs serve as natural compliant components in mechanical systems. Here, a spring-based compliant translational mechanism is studied. As shown in Fig. 11a, the spring-based compliant translational mechanism is composed of 1 rigid motion stage and 2 flexible beams. Subjected to the external force $F_o$, the mechanism starts working from the rest position where the spring is not stretched, to the stretched state where the spring is stretched. Since the structure of the mechanism is symmetrical, we can simplify the modeling by working on the half of it as

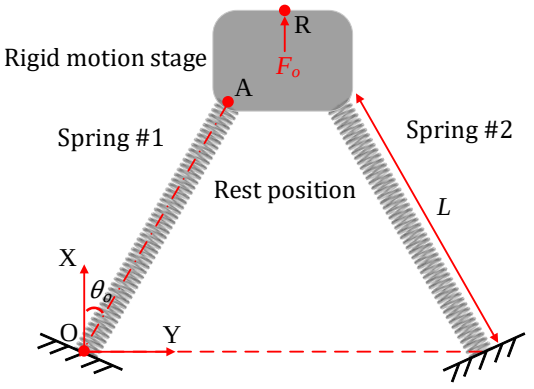


(a) Schematic diagram of a spring-based compliant translational mechanism

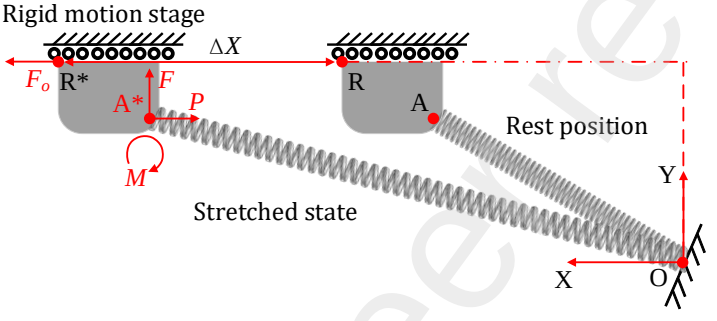


(b) Detailed force diagram of the spring-based compliant translational mechanism

**Figure 13:** Demonstration of the studied spring-based compliant translational mechanism

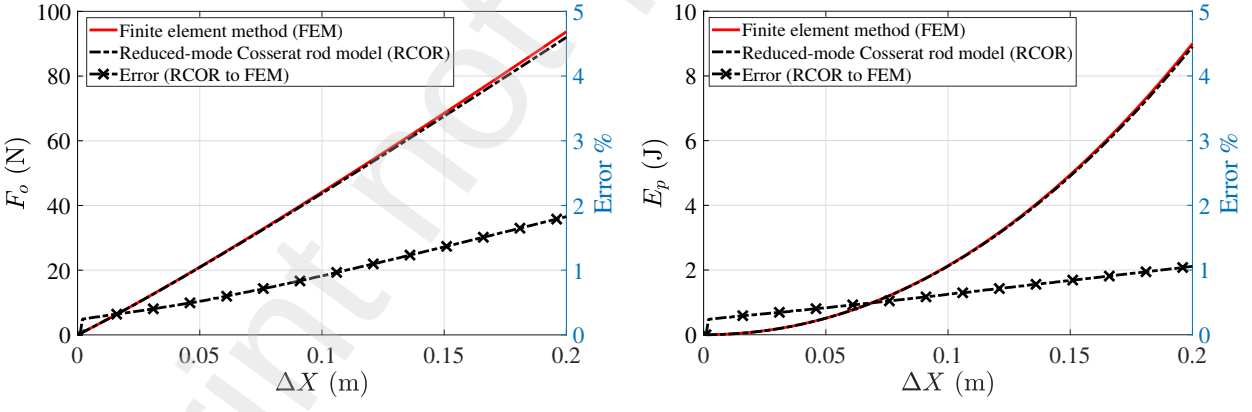


(a) $\Delta X$-$F_o$ (b) $\Delta X$-$E_p$

**Figure 14:** Numerical results of the studied spring-based compliant translational mechanism

demonstrated in Fig. 13b. The following is the dimension and material properties of the built-in flexible spring:

Number of coils ($N_t = 50$); Coil diameter ($D_c = 0.016$ m); Wire diameter ($d_w = 0.002$ m);

Helix pitch ($H_p = 0.004$ m); Helix angle ($\alpha = \arctan(\frac{d_w}{D_c}) = 0.1244$ rad); $L = N_t \times H_p = 0.2$ m;

$\theta_o = \frac{\pi}{6}$ rad; $E = 200 \times 10^9$ Pa; $\nu = 0.3$; $G = \frac{E}{2(1+\nu)}$

Then, the bending and axial stretch modulus $K_b$ and $K_s$ of the spring can calculated according to (65) and (68):

$$K_s = 50.6637 \text{ N}; \ K_b = 4.2683^{-3} \text{ N.m}$$

Therefore, we can formulate the model of the spring-based compliant translational parallelogram as a boundary value problem of an ordinary differential equation:

$$\begin{aligned} &\text{D.E.} \ \frac{\mathrm{d}^2\theta}{\mathrm{d}s^2}K_b = -P\sin\theta(s)(-\frac{\cos\theta(s)P}{K_s} + \frac{\sin\theta(s)F}{K_s} + 1) - F\cos\theta(s)(-\frac{\cos\theta(s)P}{K_s} + \frac{\sin\theta(s)F}{K_s} + 1) \\ &\text{B.C.} \ \theta(0) = \theta(L) = \theta_o \\ &\qquad \frac{\mathrm{d}\theta}{\mathrm{d}s}(L) = \frac{M}{K_b} \end{aligned} \tag{77}$$

with some constraints

$$\begin{aligned} &F_o = -2P \\ &y(L) = \int_0^L \sin\theta(s))(-\frac{\cos\theta(s)P}{K_s} + \frac{\sin\theta(s)F}{K_s} + 1)\mathrm{d}s = L\sin\theta_o \\ &\Delta X = \int_0^L \cos\theta(s))(-\frac{\cos\theta(s)P}{K_s} + \frac{\sin\theta(s)F}{K_s} + 1)\mathrm{d}s - L\cos\theta_o \end{aligned} \tag{78}$$

Then, we can numerically solve Eq. (75) and (76) using weighted residual methods [42] and Newton-Raphson method where FEM is used for verification. Here, we are interested in the relationship between $F_o$ and the displacement $\Delta X$ of the reference point R. Besides, the corresponding stored energy is also calculated by rearranging (45):

$$E_p = \int_0^L \frac{1}{2}K_s\epsilon_a^2 + \frac{1}{2}K_b\epsilon_b^2\mathrm{d}s \tag{79}$$

The numerical results are presented in Fig. 14 where the displacement $\Delta X$ and force $F_o$ & energy $E_p$ relationships are accurately calculated via RCOR. To the best of our knowledge [54], there is no other relevant methods valid for modeling flexible springs as well as flexible-spring-based compliant mechanisms. Similarly, it is promising that the proposed model can be then extended for modeling more complex compliant or flexible components as well, such as continuum manipulators and

## 6. Conclusions

Compliant mechanisms (CMs), serving as an alternative of classic rigid mechanisms, have presented several desired advantages for mechanical applications. The unique concept of transferring motion, force and energy via the elastic deflection of all these built-in flexible members has been proved valid in designing different mechanical systems. In this paper, we propose a reduced-mode Cosserat rod model to take care of all planar strains including bending, shear and stretch for modeling compliant mechanisms, sharply increasing accuracy of modeling compliant mechanisms, compared to the existing modeling methods. The feasibility of modeling compliant mechanisms via this model has also been proved. In the meanwhile, the proposed modeling strategy also present high efficiency and the potential to be extended for modeling more complex compliant structures. In the future, we will focus on introducing more efficient numerical methods to implement full-mode Cosserat rod theory for modeling more complex 3D-deflection compliant mechanisms.

## Acknowledgment

## Declaration of Competing Interest

The authors declare that they have no known competing financial interests or personal relationships that could have appeared to influence the work reported in this paper.

## References


[1] Larry L Howell. Compliant mechanisms. In 21st century kinematics. Springer, London, 2013.

[2] Larry L Howell, Spencer P Magleby, and Brian M Olsen. Handbook of compliant mechanisms. John Wiley & Sons, 2013.

[3] Nicolae Lobontiu. Compliant mechanisms: design of flexure hinges. CRC press, Boca Raton, 2020.

[4] Larry L Howell. Introduction to compliant mechanisms. Handbook of Compliant Mechanisms, pages 1–13, 2013.

[5] D Farhadi Machekposhti, N Tolou, and JL Herder. A review on compliant joints and rigid-body constant velocity universal joints toward the design of compliant homokinetic couplings. Journal of Mechanical Design, 137(3), 2015.

[6] Xin Dong, Mark Raffles, Salvador Cobos Guzman, Dragos Axinte, and James Kell. Design and analysis of a family of snake arm robots connected by compliant joints. Mechanism and Machine Theory, 77:73–91, 2014.

[7] Çağıl Merve Tanık, Volkan Parlaktaş, Engin Tanık, and Suat Kadıoğlu. Steel compliant cardan universal joint. Mechanism and Machine Theory, 92:171–183, 2015.

[8] Shorya Awtar. Synthesis and analysis of parallel kinematic XY flexure mechanisms. PhD thesis, Massachusetts Institute of Technology, 2003.

[9] Shorya Awtar and Alexander H Slocum. Closed-form nonlinear analysis of beam-based flexure modules. In ASME 2005 International Design Engineering Technical Conferences and Computers and Information in Engineering Conference, pages 101–110. American Society of Mechanical Engineers Digital Collection, 2005.

[10] Shorya Awtar, Alexander H Slocum, and Edip Sevincer. Characteristics of beam-based flexure modules. Journal of Mechanical Design, 129(6), 2007.

[11] Shorya Awtar and Alexander H Slocum. Constraint-based design of parallel kinematic xy flexure mechanisms. 2007.

[12] Shorya Awtar, Kevin Shimotsu, and Shiladitya Sen. Elastic averaging in flexure mechanisms: A three-beam parallelogram flexure case study. Journal of Mechanisms and Robotics, 2(4), 2010.

[13] Shorya Awtar and Shiladitya Sen. A generalized constraint model for two-dimensional beam flexures: Nonlinear strain energy formulation. Journal of mechanical Design, 132(8), 2010.

[14] Shixun Fan, Hua Liu, and Dapeng Fan. Design and development of a novel monolithic compliant xy stage with centimeter travel range and high payload capacity. Mechanical Sciences, 9(1):161, 2018.

[15] Ke Wu and Guangbo Hao. Design and nonlinear modeling of a novel planar compliant parallelogram mechanism with general tensural-compresural beams. Mechanism and Machine Theory, 152:1–23, 2020.

[16] Jin Qiu, Jeffrey H Lang, and Alexander H Slocum. A curved-beam bistable mechanism. Journal of microelectromechanical systems, 13(2):137–146, 2004.

[17] Huy-Tuan Pham and Dung-An Wang. A constant-force bistable mechanism for force regulation and overload protection. Mechanism and Machine Theory, 46:899–909, 2011.

[18] Yanling Tian, Kangkang Lu, Fujun Wang, Chongkai Zhou, Yue Ma, Xiubing Jing, Chengjuan Yang, and Dawei Zhang. A spatial deployable three-dof compliant nano-positioner with a three-stage motion amplification mechanism. IEEE/ASME Transactions on Mechatronics, 25(3):1322–1334, 2020.

[19] Steven D Landon. Development of deployable wings for small unmanned aerial vehicles using compliant mechanisms. Brigham Young University, 2007.

[20] RM Fowler, LL Howell, and SP Magleby. Compliant space mechanisms: a new frontier for compliant mechanisms. Mechanical Sciences, 2(2):205–215, 2011.

[21] Brian Trease and Sridhar Kota. Design of adaptive and controllable compliant systems with embedded actuators and sensors. Journal of Mechanical Design, 131(11), 2009.

[22] Myeong-Gyu Song, Hyun-Woo Baek, No-Cheol Park, Kyoung-Su Park, Taeyong Yoon, Young-Pil Park, and Soo-Cheol Lim. Development of small sized actuator with compliant mechanism for optical image stabilization. IEEE Transactions on Magnetics, 46(6):2369–2372, 2010.

[23] Peng Qi, Chen Qiu, Hongbin Liu, Jian S Dai, Lakmal D Seneviratne, and Kaspar Althoefer. A novel continuum manipulator design using serially connected double-layer planar springs. IEEE/ASME Transactions on Mechatronics, 21(3):1281–1292, 2015.

[24] Ke Wu and Gang Zheng. A comprehensive static modeling methodology via beam theory for compliant mechanisms. Mechanism and Machine Theory, 169:104598, 2022.

[25] Pier Paolo Valentini and Ettore Pennestrì. Second-order approximation pseudo-rigid model of leaf flexure hinge. Mechanism and Machine Theory, 116:352–359, 2017.

[26] Mattia Cera, Marco Cirelli, Luca Colaiacovo, and Pier Paolo Valentini. Second-order approximation pseudo-rigid model of circular arc flexure hinge. Mechanism and Machine Theory, 175:104963, 2022.

[27] Pier Paolo Valentini, Marco Cirelli, and Ettore Pennestrì. Second-order approximation pseudo-rigid model of flexure hinge with parabolic variable thickness. Mechanism and Machine Theory, 136:178–189, 2019.

[28] Matteo Verotti. Analysis of the center of rotation in primitive flexures: Uniform cantilever beams with constant curvature. Mechanism and Machine Theory, 97:29–50, 2016.

[29] Mohui Jin, Zhou Yang, Collin Ynchausti, Benliang Zhu, Xianmin Zhang, and Larry L Howell. Large-deflection analysis of general beams in contact-aided compliant mechanisms using chained pseudo-rigid-body model. Journal of Mechanisms and Robotics, 12(3):031005, 2020.

[30] Mohui Jin, Benliang Zhu, Jiasi Mo, Zhou Yang, Xianmin Zhang, and Larry L Howell. A cprbm-based method for large-deflection analysis of contact-aided compliant mechanisms considering beam-to-beam contacts. Mechanism and Machine Theory, 145:103700, 2020.

[31] Hai-Jun Su. A pseudorigid-body 3r model for determining large deflection of cantilever beams subject to tip loads. Journal of Mechanisms and Robotics, 1(2), 2009.

[32] Yue-Qing Yu, Zhong-Lei Feng, and Qi-Ping Xu. A pseudo-rigid-body 2r model of flexural beam in compliant mechanisms. Mechanism and Machine Theory, 55:18–33, 2012.

[33] Guimin Chen, Botao Xiong, and Xinbo Huang. Finding the optimal characteristic parameters for 3r pseudo-rigid-body model using an improved particle swarm optimizer. Precision Engineering, 35(3):505–511, 2011.

[34] Shun-Kun Zhu and Yue-Qing Yu. Pseudo-rigid-body model for the flexural beam with an inflection point in compliant mechanisms. Journal of Mechanisms and Robotics, 9(3), 2017.

[35] Yue-Qing Yu, Shun-Kun Zhu, Qi-Ping Xu, and Peng Zhou. A novel model of large deflection beams with combined end loads in compliant mechanisms. Precision Engineering, 43:395–405, 2016.

[36] Yue-Qing Yu and Shun-Kun Zhu. 5r pseudo-rigid-body model for inflection beams in compliant mechanisms. Mechanism and Machine Theory, 116:501–512, 2017.

[37] Robert P Chase Jr, Robert H Todd, Larry L Howell, and Spencer P Magleby. A 3-d chain algorithm with pseudo-rigid-body model elements. Mechanics based design of structures and machines, 39(1):142–156, 2011.

[38] Venkatasubramanian Kalpathy Venkiteswaran and Hai-Jun Su. Pseudo-rigid-body models of initially-curved and straight beams for designing compliant mechanisms. In International Design Engineering Technical Conferences and Computers and Information in Engineering Conference, volume 5A. American Society of Mechanical Engineers, 2017.

[39] Sinwoo Jeong and Hong Hee Yoo. Flexibility modeling of a beam undergoing large deflection using the assumed mode method. International Journal of Mechanical Sciences, 133:611–618, 2017.

[40] Christian Iandiorio and Pietro Salvini. Elasto-kinematics and instantaneous invariants of compliant mechanisms based on flexure hinges. Micromachines, 14(4):783, 2023.

[41] Horacio Ahuett-Garza, Oscar Chaides, Pedro N Garcia, and Pedro Urbina. Studies about the use of semicircular beams as hinges in large deflection planar compliant mechanisms. Precision Engineering, 38(4):711–727, 2014.

[42] Ke Wu and Gang Zheng. Insight into numerical solutions of static large deflection of general planar beams for compliant mechanisms. Mechanism and Machine Theory, 169:104598, 2022.

[43] J Awrejcewicz, AV Krysko, J Mrozowski, OA Saltykova, and MV Zhigalov. Analysis of regular and chaotic dynamics of the euler-bernoulli beams using finite difference and finite element methods. Acta Mechanica Sinica, 27:36–43, 2011.

[44] Guoyao Ma, Qi Jiang, Xiju Zong, and Jie Wang. Identification of flexural rigidity for euler–bernoulli beam by an iterative algorithm based on least squares and finite difference method. In Structures, volume 55, pages 138–146. Elsevier, 2023.

[45] Xi Song and Shi-Rong Li. Thermal buckling and post-buckling of pinned–fixed euler–bernoulli beams on an elastic foundation. Mechanics Research Communications, 34(2):164–171, 2007.

[46] Ke Wu and Gang Zheng. Solutions to large beam-deflection problems by taylor series and padé approximant for compliant mechanisms. Mechanism and Machine Theory, 177:105033, 2022.

[47] Ke Wu, Gang Zheng, and Guimin Chen. Extending timoshenko beam theory for large deflections in compliant mechanisms. Journal of Mechanisms and Robotics, 15(6):061012, 2023.

[48] Guimin Chen and Fulei Ma. Kinetostatic modeling of fully compliant bistable mechanisms using timoshenko beam constraint model. Journal of Mechanical Design, 137(2), 2015.

[49] Fulei Ma and Guimin Chen. Modeling large planar deflections of flexible beams in compliant mechanisms using chained beam-constraint-model. Journal of Mechanisms and Robotics, 8(2), 2016.

[50] Guimin Chen, Fulei Ma, Guangbo Hao, and Weidong Zhu. Modeling large deflections of initially curved beams in compliant mechanisms using chained beam constraint model. Journal of Mechanisms and Robotics, 11(1), 2019.

[51] JR Hutchinson. Shear coefficients for timoshenko beam theory. J. Appl. Mech., 68(1):87–92, 2001.

[52] Mordecai B Rubin and AH Cardon. Cosserat theories: shells, rods and points. solid mechanics and its applications, vol 79. Appl. Mech. Rev., 55(6):B109–B110, 2002.

[53] Surmont Florian and Coache Damien. Geometrically exact static 3d cosserat rods problem solved using a shooting method. International Journal of Non-Linear Mechanics, 119:103330, 2020.

[54] Mingxiang Ling, Larry L Howell, Junyi Cao, and Guimin Chen. Kinetostatic and dynamic modeling of flexure-based compliant mechanisms: a survey. Applied Mechanics Reviews, 72(3), 2020.

[55] Ke Wu and Gang Zheng. Theoretical analysis on nonlinear buckling, post-buckling of slender beams and bi-stable mechanisms. Journal of Mechanisms and Robotics, 14(3), 2022.

[56] Fedor Dmitrievich Gakhov. Boundary value problems. Elsevier, 2014.

[57] Teodor Atanackovic. Stability theory of elastic rods, volume 1. World Scientific, 1997.

[58] JW Phillips and GA Costello. General axial response of stranded wire helical springs. International Journal of Non-Linear Mechanics, 14(4):247–257, 1979.

[59] Jinwei Qiao and Na Liu. Numerical simulation of bending stiffness analysis for spring linkage applied to in-pipe robot. Mathematical Problems in Engineering, 2020:1–11, 2020.

[60] Singiresu S Rao. The finite element method in engineering. Butterworth-heinemann, 2017.

[61] Ke Wu, Gang Zheng, and Guangbo Hao. Efficient spatial compliance analysis of general initially curved beams for mechanism synthesis and optimization. Mechanism and Machine Theory, 162:104343, 2021.